PLOS COMPUTATIONAL BIOLOGY

RESEARCH ARTICLE

Cancer recurrence times from a branching process model

Stefano Avanzini, Tibor Antal*

School of Mathematics, University of Edinburgh, Edinburgh, United Kingdom

* Tibor.Antal@ed.ac.uk

Abstract

As cancer advances, cells often spread from the primary tumor to other parts of the body and form metastases. This is the main cause of cancer related mortality. Here we investigate a conceptually simple model of metastasis formation where metastatic lesions are initiated at a rate which depends on the size of the primary tumor. The evolution of each metastasis is described as an independent branching process. We assume that the primary tumor is resected at a given size and study the earliest time at which any metastasis reaches a minimal detectable size. The parameters of our model are estimated independently for breast, colorectal, headneck, lung and prostate cancers. We use these estimates to compare predictions from our model with values reported in clinical literature. For some cancer types, we find a remarkably wide range of resection sizes such that metastases are very likely to be present, but none of them are detectable. Our model predicts that only very early resections can prevent recurrence, and that small delays in the time of surgery can significantly increase the recurrence probability.

Author summary

The majority of cancer related deaths are due to the development of secondary tumors called metastases. However, the dynamics of metastases establishment and growth and their relation with the primary tumor evolution are still not clear. A standard treatment starts with the resection of the primary tumor. At this time metastases may have already formed and still be too small to be detected. The presence of only undetectable metastases poses a challenge for deciding on the follow-up therapy. These small metastases could grow to a detectable size—thus leading to a recurrence of the disease—some time after surgery. We are interested in this time until cancer relapse. We present a mathematical model of metastases formation using tools from probability theory and estimate the model parameters for five different cancer types. Our predictions for the probability of visible metastases present at surgery and the mean time to relapse when no visible metastases are found at surgery are both in agreement with clinical data.

Citation: Avanzini S, Antal T (2019) Cancer recurrence times from a branching process model. PLoS Comput Biol 15(11): e1007423. https://doi.org/10.1371/journal.pcbi.1007423

Editor: Philip K Maini, Oxford, UNITED KINGDOM

Received: February 18, 2019

Accepted: September 19, 2019

Published: November 21, 2019

Data Availability Statement: All relevant data are within the manuscript.

Funding: The authors received no specific funding for this work.

Competing interests: The authors have declared that no competing interests exist.

Introduction

Metastases develop as cancer cells disseminate from a primary tumor and establish new malignant lesions in the surrounding tissue or at other sites [1]. However, the full process of metastasis formation is much more complex and many related aspects are not yet fully understood. In particular, it is still unclear whether metastases are initiated during early or late stages of carcinogenesis (see e.g. [2–4]). These details, however, affect the chances of a patient presenting detectable or undetectable metastases at diagnosis, which in turn influence treatment strategies and prognosis. For these reasons, different authors (see e.g. [5–6] and the references therein) have proposed mathematical models to improve our understanding of the dynamics of metastasis formation.

Metastases frequently arise in cancer patients, and their occurrence greatly diminishes the chances of effective treatment. In fact, even when a therapy is initially successful, metastases often lead to relapse and are responsible for an estimated 90% of cancer related deaths [7]. Despite this common disease progression, reliable predictions for cancer recurrence rates and times are still lacking [8].

Recently, many generalizations of the Luria-Delbrück model [9] have been employed to study specific traits of tumor evolution, such as the development of drug resistance [10–13], the role of driver mutations [14, 15] and metastasis formation [5, 6, 16, 17]. Another line of research focused on temporal features, after the first stochastic model for the time to tumor onset was proposed by Armitage and Doll in their pioneering work on carcinogenesis [18]. A few decades later authors began to investigate stochastic models of tumor latency time. In particular, these works led to mathematical descriptions of optimal schedules of cancer surveillance [19, 20], cure rates [21] and cancer recurrence [22]. These models are studied in the context of survival analysis and reviewed in the excellent book of Yakovlev and Tsodikov [23].

In this paper we build a model for cancer recurrence by joining these two approaches, that is we use Luria-Delbrück type models to study cancer relapse times. In particular, we consider a deterministically growing tumor seeding metastases at a rate depending on its size [24], and model the evolution of each metastasis (or clone) as independent birth-death branching processes. A similar setup was used by Lea and Coulson to mimic mutations occurring in a growing bacterial population [25]. In our model though we interpret these mutation events (from wild-type cells to mutants) as metastasis initiation events. The distribution of mutant close sizes was studied with an exponentially growing wild-type population [26] and with more general wild-type growth function [16]. Kendall [27] also allowed the wild-type population to grow stochastically, but this extension left the mutant behavior unchanged for small initiation (mutation) rates [28, 29]. Hence in this paper we model the size of the primary tumor as a deterministic function (focusing on exponential and logistic growth as examples), while allow the seeded metastases to evolve stochastically according to branching processes.

Within this framework we study the time to cancer relapse, defined as the interval between the primary onset and the first time that any of the metastases reaches a fixed detectable size. Similar characterizations are employed in the threshold models described in [22, 23].

The rest of the paper is organized as follows: In Results we present our mathematical model of metastases initiation and growth, and derive an explicit formula for the probability distribution of the time to relapse. We then extend our model to include the resection of the primary tumor at a given time and distinguish between synchronous and metachronous metastases. In Discussion we report parameter estimates for five different cancer types (namely breast, colorectal, headneck, lung and prostate) and analyze the corresponding predictions yielded by our model. Quantitative results are compared with data collected from clinical literature. In

Material and Methods we present details about the mathematical formulation of our model and related derivations.

Results

Our mathematical characterization of the time to cancer recurrence is based on a stochastic model of metastasis formation. We first present the fundamental assumptions and features of this model, and then use them to derive the probability distribution of the time to relapse.

Model setup

We model the number of cells in the primary tumor as a deterministic function of time $n(t)$. The tumor initiates metastases at rate $\nu n(t)$, where ν is constant. We implicitly assume that all tumor cells can metastasize at the same rate. Since we make no assumptions on $n(t)$, one can define initiation at rate $\nu n(t)^\gamma$ to model scenarios where only a fraction of the primary tumor can metastasize, for example only the cells near its surface or close to blood vessels (see e.g. [6]). The initiated metastases are then modelled as independent branching birth-death processes [31], all with the same birth rate α and death rate β. We assume that they are supercritical, that is they have a positive net growth rate $\lambda = \alpha - \beta > 0$, and consequently grow exponentially for large times [31]. Exponential growth has also been observed in clinical studies [32] for untreated human lung metastases, which supports our modelling choice.

Under these assumptions each metastasis will eventually go extinct with probability $q = \beta/\alpha < 1$. The surviving ones instead grow unboundedly and will reach any given size [31]. Let M be a fixed number of cells representing the minimal detectable size of a cancerous lesion. We aim to describe the time to cancer recurrence, defined as the first time τ that any metastasis reaches the detectable size M.

The minimal detectable size M is typically very large, with estimates over 10^6 (see parameter estimations in Discussion). As the probability that a large supercritical population goes extinct is negligibly small, we assume that each metastasis survives indefinitely if it reaches M. Then, due to the splitting property of Poisson processes, the surviving metastases that eventually reach the detectable size are initiated as a non-homogeneous Poisson process $(K_t)_{t\geq 0}$ with rate $\nu(1-q)n(t)$. Here K_t denotes the number of metastases established by t, conditioned on survival. The expected number of established metastases at time t is thus

$$a_t = \mathrm{E}[K_t] = \nu(1-q)\int_0^t n(s)ds$$

and the probability that at least one is present at t is equal to

$$\mathrm{P}(K_t \geq 1) = 1 - e^{-a_t} \tag{1}$$

Surviving metastases are initiated at times $\sigma_i := \inf\{t \geq 0 : K_t = i\}$ and are described by i.i.d. birth-death processes $(S_i(s))_{s\geq 0}$, where $S_i(s)$ is the number of cells in the i-th metastasis at time s after its establishment. In particular, we have $S_i(0) = 1$ for every i. For each of these processes we define $\Theta_i := \inf\{s \geq 0 : S_i(s) = M\}$ as the time needed by the i-th established metastasis to grow to the detectable size M, counting again from its initiation. Since the processes $S_i(s)$ are independent, the hitting times Θ_i are also independent and identically distributed. As shown in Material and Methods, for M large their distribution asymptotically satisfies

$$\mathrm{P}(\Theta_i \leq t \mid \Omega_\infty^{(i)}) \sim G(t) \equiv e^{-(1-q)Me^{-\lambda t}} \tag{2}$$

where $\Omega_\infty^{(i)}$ denotes the eventual survival for the i-th metastasis. Interestingly, the distribution

$G(t)$ is of a Gumbel type, which generally describes the maximum of independent random variables with exponential (right) tail. This Gumbel type has two parameters, a and $b > 0$, and distribution function $\exp(-e^{-\frac{x-a}{b}})$. Hence, conditioned on survival, we asymptotically have $\Theta_i \sim \mathrm{Gumb}_{\max}\left(\frac{\log M(1-q)}{\lambda}, \frac{1}{\lambda}\right)$ for every i.

Time to reach detectable size

Given the definitions in the previous section, we have that the i-th metastasis reaches detectable size at time $\tau_i := \sigma_i + \Theta_i$, measured from primary onset. Metastases are initiated at time s at rate $\nu(1-q)n(s)$ and then reach the detectable size before t with probability $G(t-s)$ for $s \leq t$. Hence, the thinning property of Poisson processes yields that metastases which become detectable by time t are initiated at time s at rate $\nu(1-q)n(s)G(t-s)$. Consequently, the number of metastases detectable by t follows a Poisson process $(S_s)_{0\leq s\leq t}$ with respect to time s for a fixed t. In particular, the number S_t of such metastases established by t is thus a Poisson random variable with mean

$$b_t = \mathrm{E}[S_t] = \nu(1-q)\int_0^t n(s)G(t-s)ds \tag{3}$$

The relapse time is defined as the first time that any metastasis reaches the detectable size, $\tau := \min_i\{\tau_i\}$. Hence, τ is smaller than t if by that time at least one metastasis that becomes detectable before t is initiated, and so

$$\mathrm{P}(\tau \leq t) = \mathrm{P}(S_t \geq 1) = 1 - e^{-b_t} \tag{4}$$

A sample realisation of our model, including the relapse time τ, is depicted in Fig 1. In the large detectable size M limit, the relapse time distribution converges to a simpler form (see Material and Methods)

$$\tau - \frac{1}{\lambda}\log M \xrightarrow{d} \bar{\tau}$$

where the random variable $\bar{\tau}$ is distributed as

$$\mathrm{P}(\bar{\tau} \leq t) = 1 - \exp\left(-\nu(1-q)\int_{-\infty}^t n(t-s)e^{-(1-q)e^{-\lambda s}}ds\right) \tag{5}$$

Hence for large M the relapse time decomposes as $\tau \approx \frac{1}{\lambda}\log M + \bar{\tau}$ into a deterministic part which depends only on λ and M, plus random fluctuations described by $\bar{\tau}$. This decomposition leads to the estimate $\mathrm{E}[\tau] \sim \frac{1}{\lambda}\log M + C$ for the expected value of the relapse time, where the constant $C = \mathrm{E}[\bar{\tau}]$ can be obtained from Eq 5.

Exponential population growth

Two commonly employed primary growth functions are the exponential and the logistic ones (see e.g. [33]). These are given by $n(t) = e^{\delta t}$ and $n(t) = \frac{Ke^{\delta t}}{K+e^{\delta t}-1}$, respectively, where δ denotes the primary tumor net growth rate and K a carrying capacity. Relapse time densities for these two growth types and different initiation rates are shown in Fig 2. We observe that as ν increases, the logistic distributions converge to the exponential ones (see Material and Methods for more details). Moreover, for all our parameter estimates our model predicts the same results with these two growth types. The reason is that the metastases determining the time to relapse are initiated during the early phase of tumor evolution which is almost exponential even for a

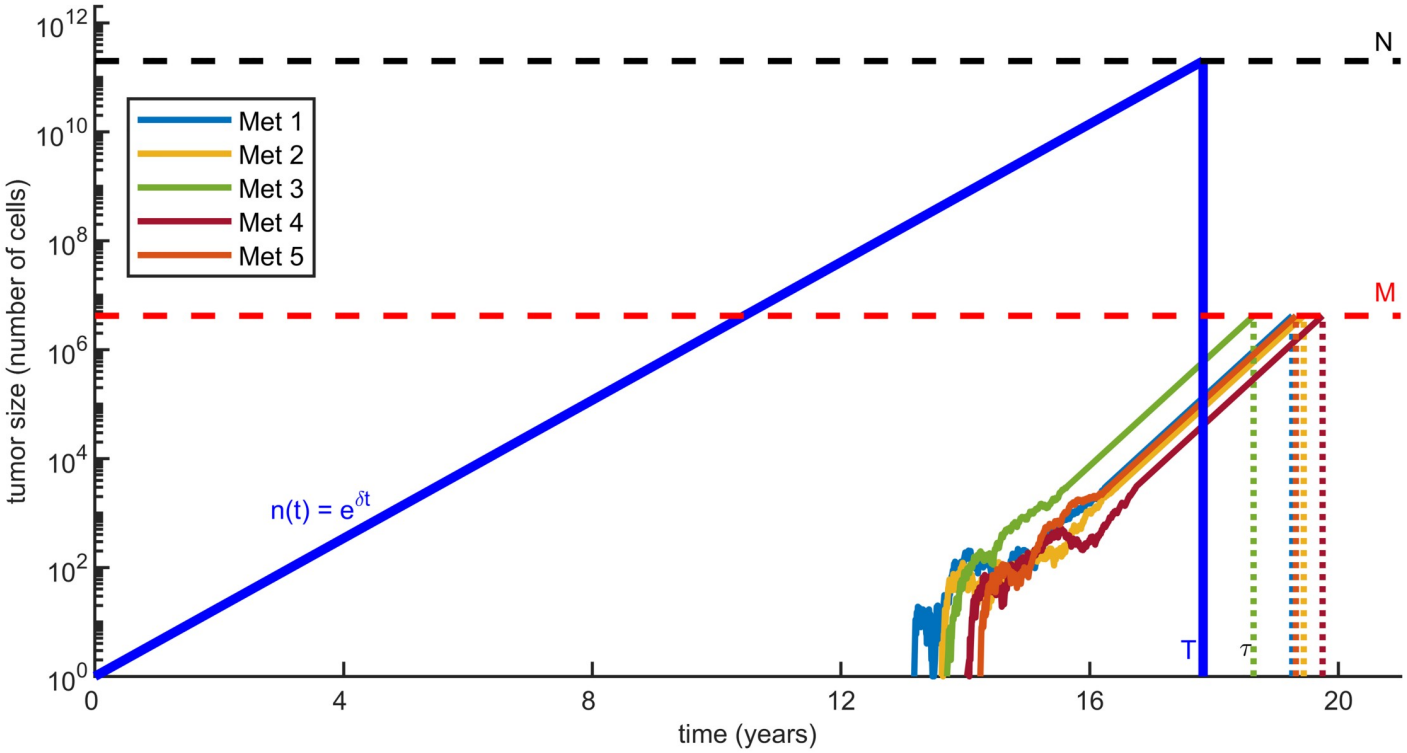

Fig 1. Sample realisation of the model obtained by simulations. The primary tumor grows according to a deterministic exponential function $n(t)$—depicted by the blue line. It initiates distant metastases at rate $\nu n(t)$, and each of them grows as an independent branching process (only the first five are plotted). The first time τ that any of these metastases reaches a minimal detectable size M is defined as the time to cancer relapse. Also, the primary tumor is surgically removed at a given time T, when it is made of $N = n(T)$ cells. In the realisation shown, the third established metastases (green curve) is the first to reach detectable size, and hence determines the time to cancer relapse τ. Based on clinical data (summarized in Table 1), we estimated model parameters (summarized in Table 2), and here we use those for colorectal cancer, with $N = 2 \times 10^{11}$. Note that a similar illustration for metastasis formation appears in [30].

https://doi.org/10.1371/journal.pcbi.1007423.g001

logistic growth. Therefore, from now on we will focus on exponentially growing primary tumors. Exponential growth has the additional advantage that if only a portion of primary cells can metastasize and their number is proportional to $n(t)^\gamma$ (say only cells close to the surface of a spherical tumor for $\gamma = 2/3$), then this would be equivalent to changing the primary net growth rate, that is using $n(t) = e^{\gamma\delta t}$.

Since the initiation rate ν is by far the slowest rate in our model, here we study in detail the most relevant case, that is the small ν limit for an exponentially growing tumor. The deterministic part of the relapse time remains $\frac{1}{\lambda}\log M$, but interestingly the fluctuations $\bar{\tau}$ are distributed as

$$\bar{\tau} \sim \mathrm{Gumb}_{\min}\left(-\frac{1}{\delta}\log\frac{\nu(1-q)^{1-\frac{\delta}{\lambda}}\Gamma\left(\frac{\delta}{\lambda}\right)}{\lambda}, -\frac{1}{\delta}\right) \tag{6}$$

This Gumbel distribution describes the minimum of independent random variables with exponential (left) tail, has two parameters a and $b < 0$ and distribution $1 - \exp(-e^{-\frac{x-a}{b}})$. Parameter a describes a shift in the distribution, and since $a \sim \log \nu$, it explains the equal spacing between the densities in Fig 2 for logarithmically-spaced values of the initiation rate. Also notice that these curves are left skewed, as it is expected from the Gumbel for the minimum.

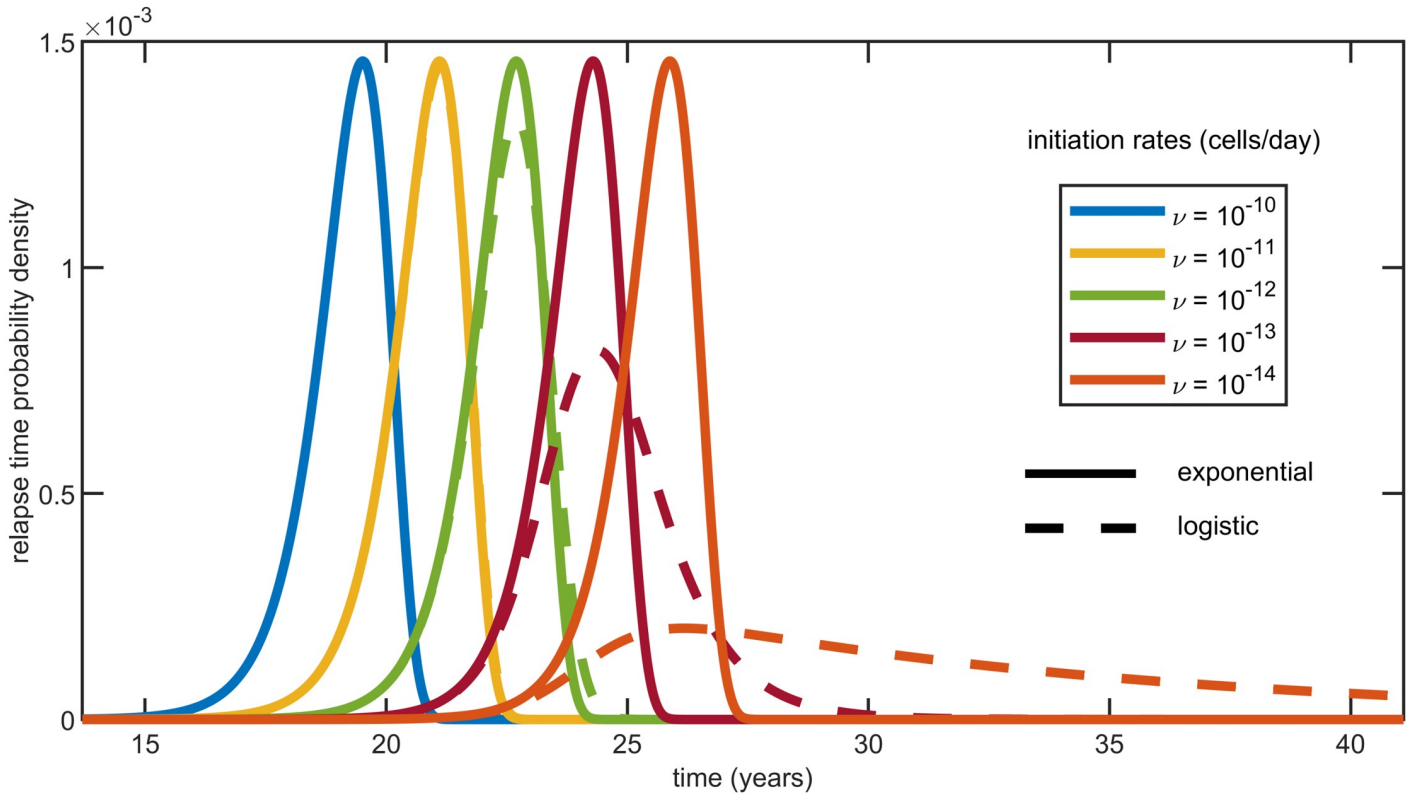

Fig 2. Relapse time densities $f_\tau(t) = \frac{d}{dt}\,\mathrm{P}(\tau \le t)$ computed from Eq 4 for logistic and exponential primary growths and $\nu = 10^{-10}, 10^{-11}, 10^{-12}, 10^{-13}, 10^{-14}$ cells/day from left to right. Using parameter estimates for colorectal cancer (see Table 2), the logistic densities (dashed lines) converge to the corresponding exponential ones as the initiation rate increases. Furthermore, in the exponential case and for all the above values of ν, the densities derived from Eq 4 and their approximation obtained from Eq 6 are indistinguishable.

https://doi.org/10.1371/journal.pcbi.1007423.g002

On the other hand, the Gumbel for the maximum—which describes the fluctuations of the time to detection starting from a single initial cell—is right skewed.

For small initiation rates ν and large detectable sizes M, the mean relapse time is approximately given by

$$\mathrm{E}[\tau] \approx \frac{1}{\lambda}\log M + \frac{1}{\delta}\log\frac{\delta}{\nu} + C\,, \qquad C = -\frac{1}{\delta}\left(\log\frac{\delta(1-q)^{1-\frac{\delta}{\lambda}}\Gamma\left(\frac{\delta}{\lambda}\right)}{\lambda} + \gamma_E\right) \tag{7}$$

where $\gamma_E \approx 0.5772$ denotes the Euler-Mascheroni constant. As shown by Fig 3, this expression fits simulations even for relatively large values of ν and small values of M. Eq 7 highlights a simple dependence of the mean relapse time $E[\tau]$ on M and ν. In Material and Methods we also compute the mean time to detectability of the first established metastasis, $E[\tau_1]$, where $\tau_1 = \sigma_1 + \Theta_1$ is equal to the sum of the first initiation time and the hitting time to M. Interestingly $E[\tau_1]$ has the same M and ν dependence shown in Eq 7, but the constant term $\tilde{C}$ is different. For example, using the parameter estimates for colorectal cancer (see Table 2) we find $C \approx 250$ and $\tilde{C} \approx 309$. The reason for this difference is that even in the small ν—large M limit, later established metastases can outrun the earlier ones in reaching M first.

While the mean relapse time τ shows logarithmic increase in terms of M and δ/ν, its variance stays constant, $\mathrm{Var}(\tau) = \pi^2/(6\delta^2)$, see Eq 15. Hence, due to the slow logarithmic growth of

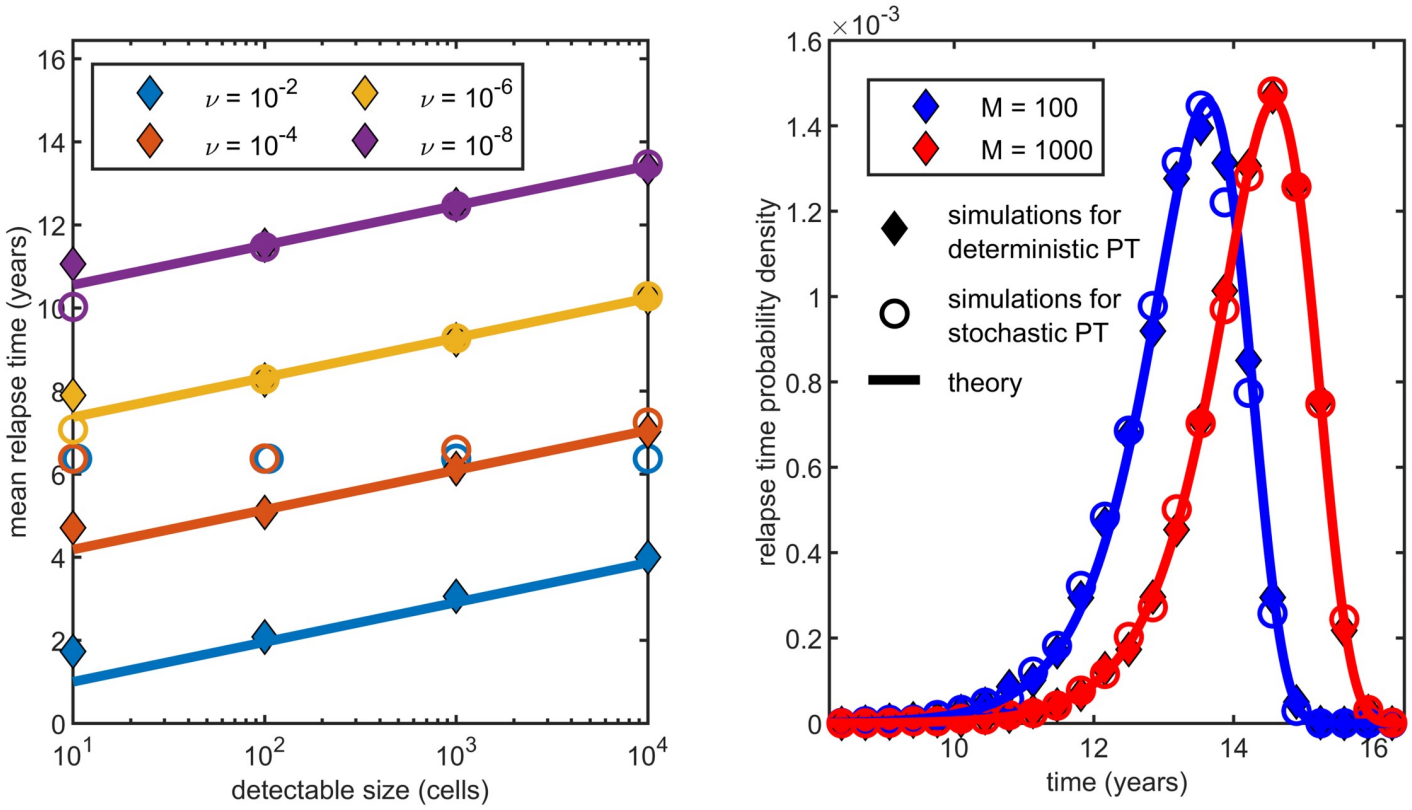

Fig 3. Relapse time distribution for an exponentially growing primary tumor using parameter estimates for colorectal cancer (see Table 2). Symbols represent simulation results for a deterministic (diamonds) or a stochastic primary growth (circles, see Discussion at the end of the parameter estimation section), while solid lines correspond to the theory in the small ν—large M limit. On the left, each starred dot denotes the mean of 1000 simulations, while lines represent the theoretical expectation given by Eq 7. These match the simulated means well for values of $\nu = 10^{-6}$ or less. On the right, the relapse time densities derived from Eq 14 yield a good approximation of the simulated data (10000 simulations per curve) for $M = 100$ or greater for both deterministic and stochastic primary growth.

https://doi.org/10.1371/journal.pcbi.1007423.g003

the mean, the fluctuations of the relapse time stay relevant even for large detection sizes and small mutation rates.

Relapse time with resection

Surgery is still the most common and effective type of treatment for solid tumors, although often used in combination with other kind of therapies (see e.g. [34]). However, how the time of resection affects prognosis, and in particular the estimation of the time to relapse, is still unclear. In order to investigate this question in a theoretical framework, we now embed surgery in our model and study how it changes the distribution of the time τ to relapse. Let us assume that at a given moment after detection a primary solid tumor is surgically removed. This event can be mathematically implemented in our model by considering a resection time T such that $n(t) \equiv 0$ for $t \geq T$. In particular, this implies that after T no metastases can be initiated. The number of metastases already established at resection is equal to K_T, and their size distribution is given in [16]. The distribution of the time τ to relapse can then be expressed exactly as in Eq 4, however here τ is not a proper random variable. In fact, as $\int_0^\infty n(s)ds = \int_0^T n(s)ds < \infty$, there is a positive probability that no metastasis will ever occur (notice that from this point of view our framework can be seen as a cure model—see e.g. [35]) and in this case we set $\tau = \infty$. The distribution of the relapse time conditioned on at least one

metastasis being established by resection is simply

$$\mathrm{P}(\tau \le t \mid K_T \ge 1) = \frac{\mathrm{P}(\tau \le t)}{\mathrm{P}(K_T \ge 1)} = \frac{1 - e^{-b_t}}{1 - e^{-a_T}} \tag{8}$$

where we used that a relapsing metastasis had to be initiated before resection, that is $\{\tau \le t\} \subset \{K_T \ge 1\}$. This conditional distribution for different resection times is depicted in Fig 4. In this and following figures, the resection time is shown at the bottom of the figure, and the corresponding resection size $N = e^{\delta T}$ is shown on the top. As $T \to 0$ all metastases have to be initiated close to time zero, so the relapse time becomes the time to reach size M from a single cell, which has the Gumbel distribution for the maximum given by Eq 2. If we then increase the resection time, the conditional densities shift to the right by the same amount. Finally, as $T \to \infty$ the relapse time distribution converges to the case without resection

$$\mathrm{P}(\tau \le t \mid K_T \ge 1) \to \mathrm{P}(\tau \le t)$$

The fluctuations for the unconditional distribution follow a Gumbel type for the minimum, as per Eq 6. Hence, as time increases, the relapse time distribution turns from a right-skewed Gumbel to a left-skewed Gumbel.

Note that the densities in Fig 4 become indistinguishable from the large time limit as $P(K_T \ge 1)$ approaches one. The reason is that by this time metastases have probably already

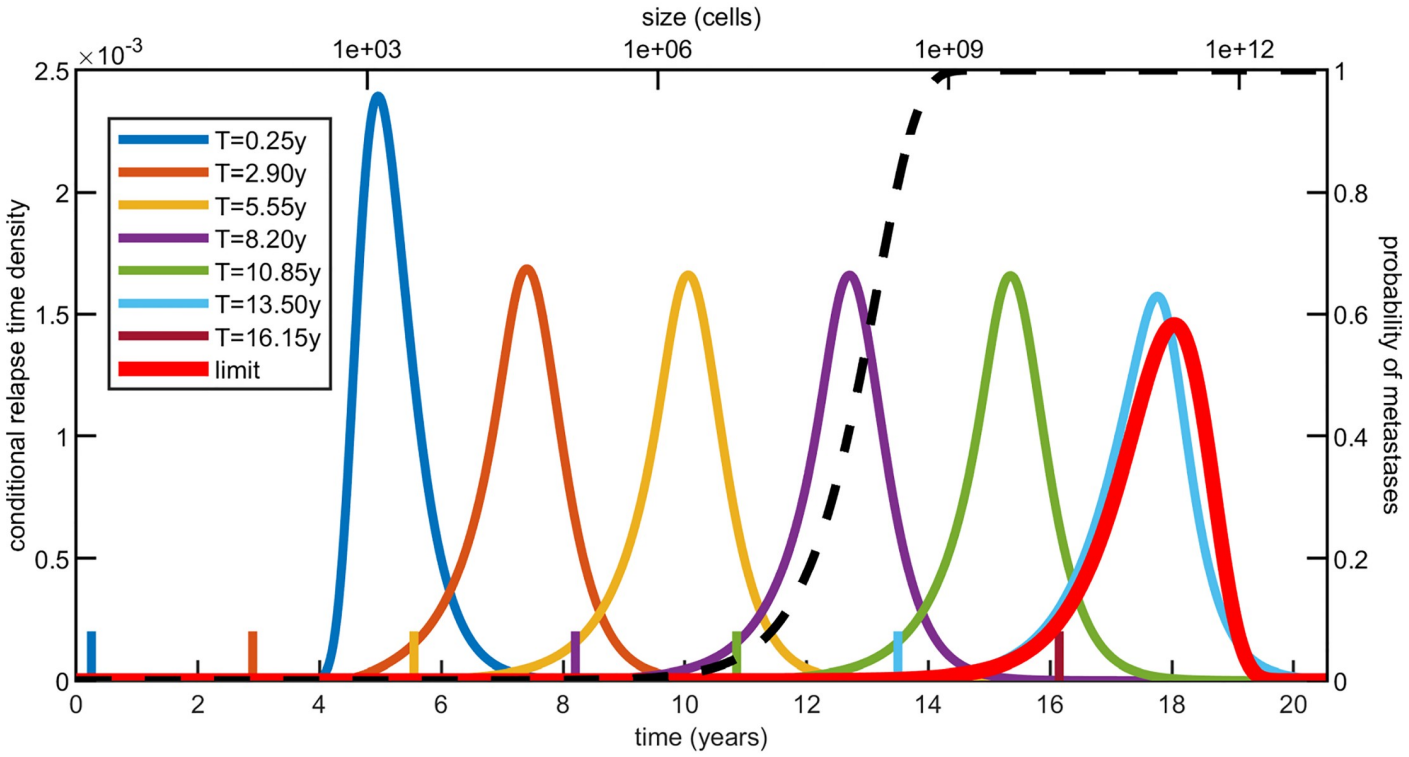

Fig 4. Relapse time densities $f_\tau(t|K_T \ge 1)$ conditioned on at least one metastasis initiated by the time of resection T. For different values of T, marked with ticks of corresponding colors, these densities are computed by differentiating Eq 8. As T becomes larger, the probability of metastases being established before resection (see Eq 1) increases and the conditional relapse time densities converge to the red limit one. Here we have used parameter estimates for colorectal cancer (see Table 2), $n(t) = e^{\delta t}$ and 7 equally spaced resection times between 0.25y and 16.15y. The curves for $T > 15$y look identical to the limit density.

https://doi.org/10.1371/journal.pcbi.1007423.g004

been initiated and one of the early established ones is likely to relapse first. This suggests that only early enough resection times change the behaviour of the model. For example in the case of colorectal cancer, according to Fig 4, only resections of tumors smaller than 10^9 cells affect the time to recurrence.

Right skewed densities are often chosen to fit probability distributions arising in survival analysis. This is due to the fact that most survival data suffer from right censoring [36], where only a lower bound is known for data points. Looking at the densities in Fig 4, though, we can see both left and right skewed distributions. While a few survival datasets are negatively skewed [37], cancer relapse times are typically right censored as a consequence of limited follow-up and patients decease before relapse (see e.g. [38]). However, our model does not take into account any of these events. Furthermore [39] recently proposed a model for the estimation of screening times for colorectal cancer based on the observation that some datasets suffer from left censoring as well.

Metastasis classification

If the resection is successful and the primary tumor is completely removed, the therapy can still fail due to the formation of metastases. For this reason, it is common practice to start looking for detectable metastases several weeks before the surgery. In this section we thus want to characterize the metastases which are detectable at a given time and those which are not.

In general, for a fixed time t, the metastasizing process $(K_s)_{0\leq s\leq t}$ can be split into two independent Poisson processes $(S_s)_{0\leq s\leq t}$ and $(M_s)_{0\leq s\leq t}$ describing the initiation of metastases which reach size M before or after t, respectively. Following the same argument we used to derive the relapse time distribution, we obtain that

$$S_t \sim \text{Pois}(b_t), \qquad M_t \sim \text{Pois}(c_t)$$

where

$$c_t = a_t - b_t$$

In particular, we have that the events $\{\tau > t\}$ and $\{S_t = 0\}$ are equivalent. We also stress that the definitions above naturally extend to the case of a primary resection, by simply redefining $n(t)$ to be zero after the resection time T.

Now, despite an ongoing discussion on the following nomenclature (see e.g. [40]), in the rest of the paper we will call a metastasis synchronous if it reaches the detectable size M before or up to the time of resection, and metachronous otherwise (hereby the choice of notation S_t and M_t). These characterizations immediately allow us to estimate the probability of some clinically relevant events. The probability of no synchronous metastases is equal to

$$\text{P}(S_T = 0) = \text{P}(\tau > T) = e^{-b_T} \tag{9}$$

Also, under this condition, relapse is not certain: the probability that at least one metastasis was initiated given that there are no visible ones at resection is

$$P(K_T \geq 1 \mid S_T = 0) = \text{P}(M_T \geq 1) = 1 - e^{-c_T} \tag{10}$$

since S_T and M_T are independent. In next section we will study the above and related quantities in greater detail.

Discussion

In this section we compare the predictions provided by our model with clinical data collected for different cancer types. To this purpose, we first need to estimate the parameter values for each of these cancer types.

Parameter estimation

The net growth rates of the primary and metastatic tumors, δ and λ, are inferred from the corresponding tumor volume doubling times (denoted DT_{pt} and DT_m, respectively) as

$$\delta = \log 2/DT_{pt}\,, \quad \lambda = \log 2/DT_m$$

These times have been studied by many authors, starting from the influential papers of [32, 41, 42]. Many authors still refer to these early works, although in some case more recent estimates are available. Colorectal, breast and lung cancers are the most frequently studied. Furthermore, more papers focus on primary doubling times than on metastatic ones.

Similarly, the birth rate α is derived from the potential doubling time T_{pot}, defined as the average time between cell divisions in the absence of cell death [43–45]. In this case we simply use the estimation

$$\alpha = 1/T_{pot}$$

Note that some authors (see e.g. [46]) define instead T_{pot} as the tumor doubling time in absence of cell death. While in this paper we employ the former definition, the latter would simply yield a factor log 2 in the formula above.

As for the primary tumor size N at resection, many studies report data on the primary maximum diameter, allowing for ellipsoidal forms. However, given the relatively small tumor volume and the wide interpatient variability, we assume a spherical shape and estimate d_{pt} from the corresponding typical range. By also assuming 10^9 cells per cm^3, the primary size at resection (expressed in number of cells) is thus estimated as $N = \frac{1}{6}\pi d_{pt}^3 10^9$.

Table 1 summarizes typical ranges of these quantities for five different cancer types, together with the estimates we picked for our model and the corresponding literature references. Difficulties in distinguishing between primary and secondary tumors or in tracking down the primary origin of a metastatic cancer could in principle affect some of these data, but the wide range and multiple references reported reduce the potential impact of this effect.

Notice that by estimating the rates λ and α we also infer values for the death rate $\beta = \alpha - \lambda$ and the extinction probability $q = 1 - \lambda/\alpha$. For the two remaining parameters, namely the initiation rate ν and the minimal detectable size of a metastasis M, we use common estimates across different cancer types. Various studies report a lowest detectable tumor diameter of 0.2cm for different cancer types (see e.g. [90–92]), corresponding to $M \approx 4.19 \times 10^6$ cells. Moreover, several papers argue that the first metastases are likely to be established long before the detection of the primary tumor (see for example [54] and the references therein). In particular, the review of the progression model for metastases formation in [24] reports that dissemination starts when the primary diameter is between 0.1 and 0.4cm. We thus consider the primary tumor size at the expected time of the first metastasis initiation and estimate it to be $e^{\delta \mathrm{E}[\sigma_1]} = 10^8$ cells, corresponding to a diameter of about 0.58cm. Hence, by using the results in

Table 1. Typical ranges of volume doubling times for the primary tumor (DT_{pt}) and metastasis (DT_m), tumor potential doubling time (T_{pot}) and tumor diameter at resection (d_{pt}) for breast, colorectal, headneck, lung and prostate cancer.

Cancer type	Parameter	Typical range	Estimate	References
Breast	DT_{pt} (days)	103 – 353	210	[47–52]
	DT_m (days)	85 – 199	105	[53, 54]
	T_{pot} (days)	8 – 35	15	[44, 55]
	d_{pt} (cm)	1.4 – 3	2.5	[56–58]
Colorectal	DT_{pt} (days)	130 – 438	175	[59–61]
	DT_m (days)	45 – 155	105	[54, 62–64]
	T_{pot} (days)	3 – 4	4	[55, 65]
	d_{pt} (cm)	3.5 – 5.1	4.5	[59, 61, 66, 67]
Headneck	DT_{pt} (days)	15 – 256	84	[68, 69]
	DT_m (days)	9.5 – 320	56	[70, 71]
	T_{pot} (days)	1 – 14	4	[65, 72]
	d_{pt} (cm)	1.3 – 4	2.8	[73, 74]
Lung	DT_{pt} (days)	22 – 269	168	[54, 75–78]
	DT_m (days)	32 – 98	56	[42, 79]
	T_{pot} (days)	2 – 17.5	2.5	[75, 80]
	d_{pt} (cm)	1.7 – 4.1	2	[77, 81, 82]
Prostate	DT_{pt} (days)	36 – 1080	392	[83–85]
	DT_m (days)	29 – 213	98	[85, 86]
	T_{pot} (days)	15.2 – 97.8	34	[84, 87]
	d_{pt} (cm)	0.1 – 2.9	1.2	[88, 89]

https://doi.org/10.1371/journal.pcbi.1007423.t001

Material and Methods, we set

$$v = \frac{\delta e^{-\gamma_E}}{1-q} e^{-\delta \mathrm{E}[\sigma_1]}$$

Finally, the carrying capacity for the logistic primary growth studied in Fig 2 is set to $K = 10^{12}$ [24, 93]. Overall, we thus found estimates for the following input vector

$$(DT_{pt}, DT_m, T_{pot}, d_{pt}, d_m, e^{\delta \mathrm{E}[\sigma_1]})$$

and used them as described above to derive values for our model parameters, i.e.

$$(\delta, \lambda, v, q, N, M)$$

Such estimates are summarized in Table 2.

Before we proceed to study our model predictions, let us further discuss the assumption of a deterministic primary tumor growth function. Firstly, as we just showed, the only data we

Table 2. Parameter estimates for the primary net growth rate δ, the metastatic net growth rate λ, the initiation rate v, the extinction probability q, the primary tumor size at resection N and the minimal detectable size M.

	Breast	Colorectal	Headneck	Lung	Prostate
δ (cells/day)	0.0033	0.0040	0.0083	0.0041	0.0018
λ (cells/day)	0.0066	0.0066	0.0124	0.0124	0.0071
v (cells/day)	1.87×10^{-10}	8.42×10^{-10}	9.36×10^{-10}	7.49×10^{-10}	4.13×10^{-11}
q	0.9010	0.9736	0.9505	0.9691	0.7595
N (cells)	8.18×10^9	4.77×10^{10}	1.15×10^{10}	4.19×10^9	9.05×10^8
M (cells)	4.19×10^6	4.19×10^6	4.19×10^6	4.19×10^6	4.19×10^6

https://doi.org/10.1371/journal.pcbi.1007423.t002

found to infer the rate of growth of a primary tumor refer to doubling times, whose notion implicitly assumes an exponential growth. For this reason we focus here on growth functions that (at least in their early stages) show an exponential behaviour. Other growth functions, for example $n(t) = ct^3$ for spherically growing tumours or $n(t) = c' t^2$ for tumors with active cells only around the surface, could be studied when more data becomes available. Secondly, one could model not just the metastases but also the primary tumor growth as a branching process to account for further stochastic effects. However, due to the large tumor size at resection a branching process model would predict an almost perfect exponential growth around resection time. For this reason we set $n(t) = e^{\delta t}$, which then determines the initial time $t = 0$. Note that the tumor is not initiated precisely at $t = 0$, but that time is distributed according to a Gumbel distribution, analogously to the results in the Single type process section in Materials and methods. Since the initiation time is not accessible experimentally anyway, for simplicity we use this above definition for $t = 0$. In order to justify the exponential deterministic approximation for the primary size, we performed simulations where we modelled the primary tumor as a branching process as well. We found that for initiation rates of $\nu = 10^{-5}$ or less (and all other parameters set for colorectal cancer) the exponential approximation of the primary causes less than a few percent error in the relapse time distribution (see Fig 3). The relationship between stochastic and deterministic wild type populations has been studied rigorously in [29].

Model predictions

Now that we have estimated the parameters of our model in Table 2, we are in position to study its predictions and compare them to clinical data.

Let us start by analyzing the simplest predictions of the model, which are about the presence of synchronous and metachronous metastases. Fig 5 shows the probability of initiated metastasis by resection $\mathrm{P}(K_T \geq 1) = 1 - e^{-a_T}$ (Eq 1), and the probability of visible metastasis by resection $\mathrm{P}(S_T \geq 1) = 1 - e^{-b_T}$ (Eq 4) as functions of the resection time T, for five different cancer types. that, obviously, the probability of having initiated metastasis is always higher than the probability of having visible metastasis at resection. For all five cancer types considered, one or more metastases have likely been initiated by the time the primary tumor reaches about 8.2×10^8 cells (diameter 1.16cm). While this value is similar across different primary types (as a consequence of the parameters estimation procedure), the results for the probability of synchronous metastases vary widely. For breast, colorectal, headneck, lung and prostate cancer, Table 3 reports primary tumor sizes at which synchronous metastases might start to appear and are likely to be present, respectively (expressed both in terms of number of cells and tumor diameter). By comparing these values to typical resection sizes in Table 1, we find that detecting metastases at resection is very likely for lung and prostate cancer and rare for headneck primary tumors.

One of the most challenging scenarios for the development of an effective treatment is when there are only undetectable metastases present. In our framework this scenario corresponds to the event

$$U_T \coloneqq \{K_T \geq 1, S_T = 0\} \tag{11}$$

which has probability (see Eqs 9 and 10)

$$\begin{aligned} \mathrm{P}(U_T) &= \mathrm{P}(M_T \geq 1, S_T = 0) = \mathrm{P}(M_T \geq 1)\,\mathrm{P}(S_T = 0) \\ &= e^{-b_T} - e^{-a_T} = \mathrm{P}(K_T \geq 1) - \mathrm{P}(S_T \geq 1) \end{aligned} \tag{12}$$

Because of the last identity, the probability of established and all metachronous metastases can be read out from Fig 5 as the difference of the two curves. There, the shaded areas highlight

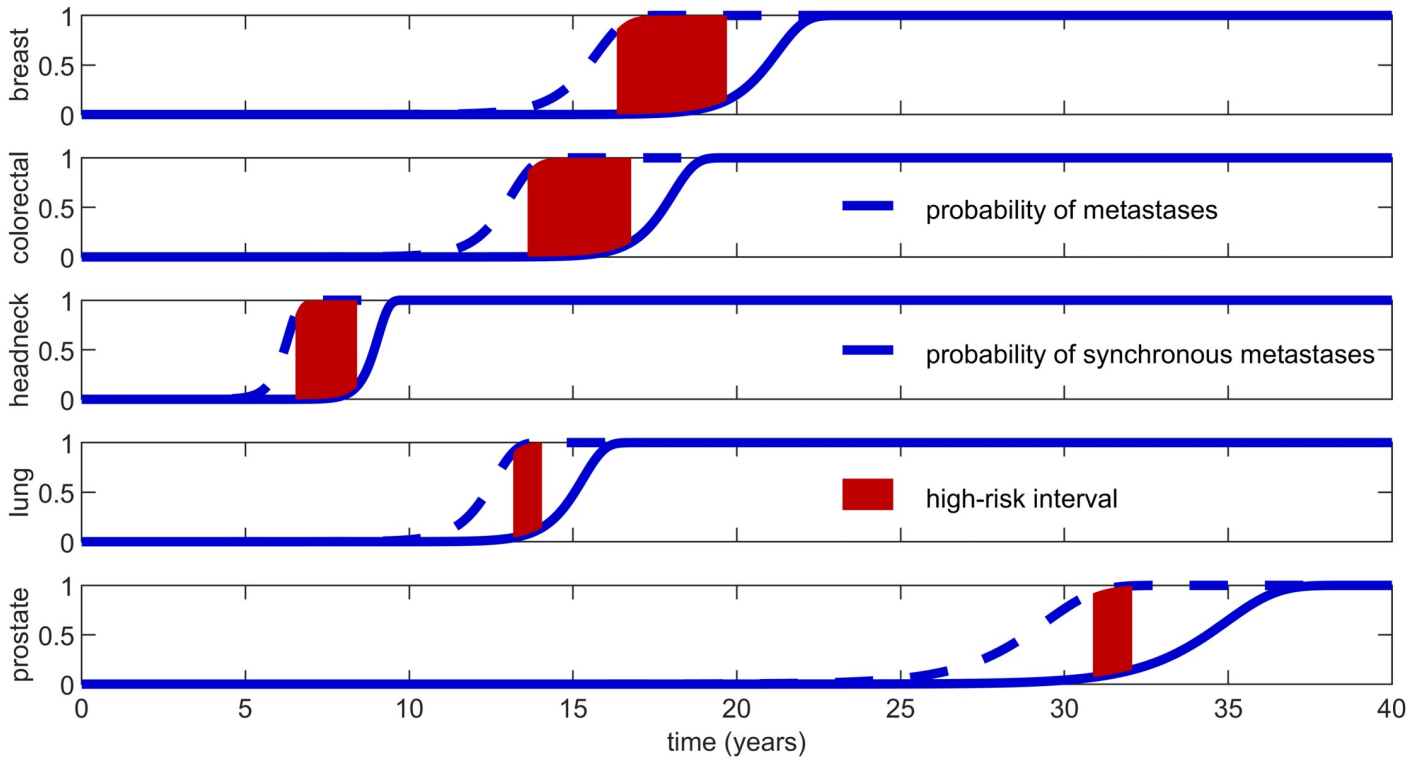

Fig 5. Probability of extant metastases, $P(K_T \geq 1)$, dashed curve computed from Eq 1, and synchronous metastases, $P(S_T \geq 1)$, solid curve computed from Eq 4. These probabilities are plotted as functions of the resection time T for five different cancer types. The primary tumor size at resection is $N = e^{\delta T}$ and thus depends on the primary net growth rate. These resection sizes are discussed in Table 3. For each cancer type, the shaded areas highlight resection time intervals leading to a probability higher than 85% of established and all undetectable metastases. Using the parameter estimates from Table 2, the widths of these intervals are 3.41, 3.17, 1.92, 0.94, 1.19 years for breast, colorectal, headneck, lung and prostate cancer respectively.

https://doi.org/10.1371/journal.pcbi.1007423.g005

intervals of resection times yielding $P(U_T) > 85\%$. These intervals, often referred to as high-risk period [94], are especially wide for breast, colorectal and headneck cancers. The reason is that these cancer types have a lower ratio of metastatic over primary net growth rates, so metastases take longer to grow to visible size. Hence, although for these cancer types metastases grow slower, which improves prognosis, they stay undetectable for longer, which poses a challenge for diagnosis. The estimated resection sizes given in Table 1 fall within or close to these ranges ($P(U_T)$ equal to 93.87%, 79.83%, 98.35%, 66.04% and 85.85% for the five primary tumor types studied, respectively). In general, by assuming that the primary tumor diameter at resection fits a normal distribution (with mean computed as the mean of d_{pt} and variance set so that 95% of the observations belong to its typical range, see Table 1) we estimate that resections for breast and headneck cancers fall in the high-risk window 99.8% and 99.58% of the

Table 3. Resection sizes of the primary tumor which yield a 1% and 99% probability of synchronous metastases, respectively. For each cancer type considered, these sizes are computed with the parameter values in Table 2 and expressed both in terms of number of cells, N, and tumor diameter, d.

		Breast	Colorectal	Headneck	Lung	Prostate
$P(S_T \geq 1) > 0.01$	N	1.32×10^9	2.13×10^9	7.03×10^9	1.03×10^8	6.27×10^7
	d	1.36	1.60	2.38	0.58	0.49
$P(S_T \geq 1) > 0.99$	N	6.03×10^{11}	9.88×10^{11}	3.22×10^{12}	4.65×10^{10}	2.89×10^{10}
	d	10.48	12.36	18.32	4.46	3.81

https://doi.org/10.1371/journal.pcbi.1007423.t003

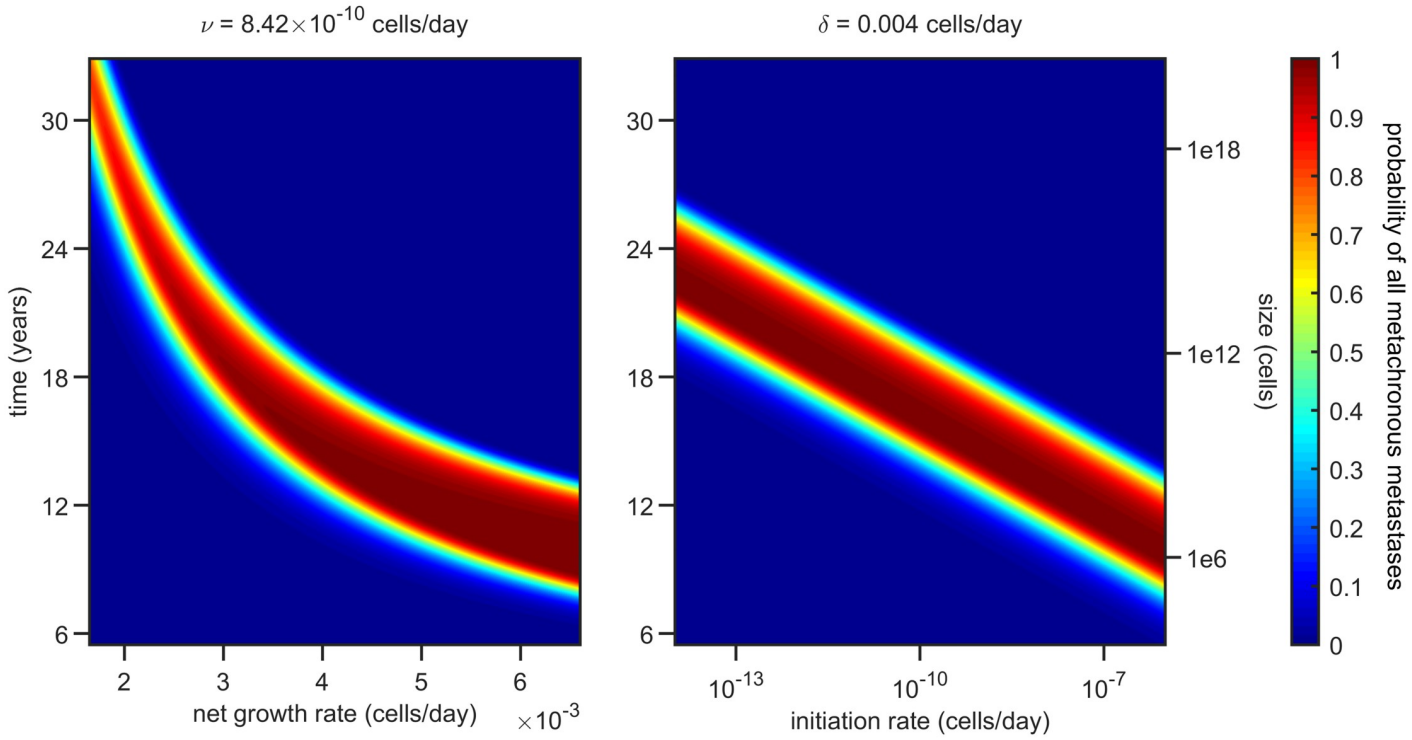

Fig 6. Probability of established and all metachronous metastases—$P(U_T)$, as given by Eq 12—plotted as a function of T and δ (left panel) and of T and ν (right panel). The parameter estimates used are those for colorectal cancer reported in Table 2. The plots show that the width of the high-risk interval—the range of resection times such that $P(U_T)$ is high—stays roughly constant for most parameter values. This width (about 3 years) shrinks only for metastases growing significantly faster than the primary tumor that initiated them.

https://doi.org/10.1371/journal.pcbi.1007423.g006

times respectively, followed by colorectal (24.67%), prostate (13.41%) and lung (0.69%) cancers.

In order to check how robust the presence of a wide high-risk interval is, we plotted in Fig 6 the probability of having only undetectable metastasis at detection, $P(U_T)$, for different values of the primary net growth rate δ and of the initiation rate ν. Other parameters are taken for colorectal cancer. The width of the high-risk interval is constant with respect to ν, and shrinks only as the ratio between the primary and metastatic net growth rate becomes very small. The same qualitative behaviour can be obtained with the parameter estimates for the other cancer types. As most metastases grow up to two times faster than the primary tumor they originated from [24], our model suggests that for a wide choice of parameters there is a substantial range of resection sizes that lead to a high probability of established and all undetectable metastases.

Next, we ask how such a probability, $\mathrm{P}(U_T)$, influences the time to cancer recurrence. The conditional distribution of the relapse time τ becomes

$$\mathrm{P}(\tau \leq t \mid U_T) = \frac{\mathrm{P}(T < \tau \leq t \mid K_T \geq 1)}{\mathrm{P}(T < \tau \mid K_T \geq 1)} = \frac{e^{-b_T} - e^{-b_t}}{e^{-b_T} - e^{-a_T}}$$

for $t \geq T$, where we used the definition of U_T (see Eq 11) and Eq 8. From this distribution we compute the expected relapse time measured from resection and conditioned on U_T, $E[\tau - T|U_T]$. This expectation and the probability $\mathrm{P}(U_T)$ are plotted in Fig 7. We see that for resection sizes smaller than 10^8 cells the relapse occurs on average between 4 and 5 years after resection, independently of the primary size. For resection sizes around 10^8 cells, undetectable metastases become likely to be present and $E[\tau - T|U_T]$ starts to decrease with tumor size. At

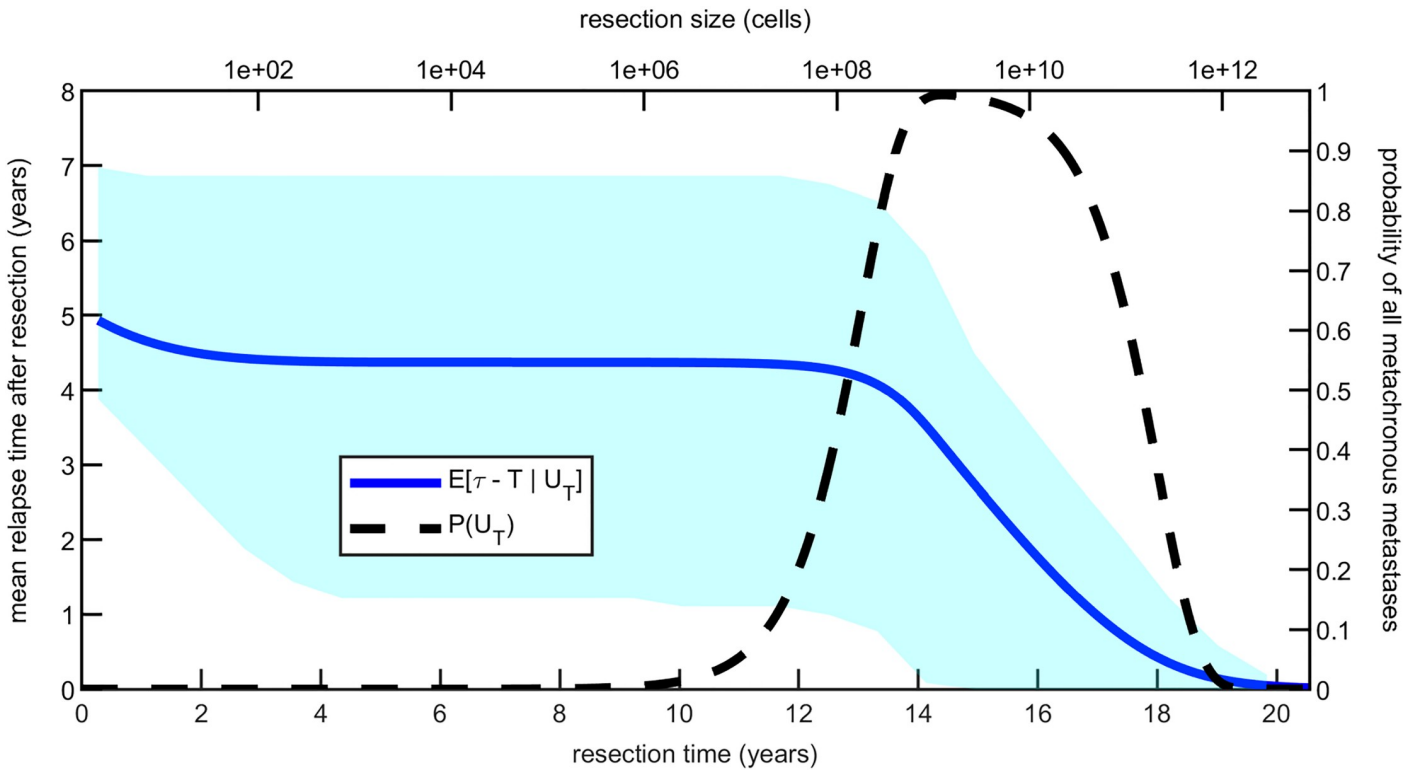

Fig 7. Expected relapse time measured from resection, conditioned on extant but all undetectable metastases (blue curve). The dashed line and the light blue shaded area show $P(U_T)$ and how spread is the conditional relapse time distribution, respectively. The parameter estimates used are those for colorectal cancer reported in Table 2. For resection times close to zero this conditional expectation coincides with that of the Gumbel distribution given by Eq 14, at about 5 years. As T starts to increase $E[\tau - T|U_T]$ reflects the convergence highlighted for Fig 4, first slightly decreasing and then staying constant around 4.4 years. Finally, when the resection time falls into the high-risk window, the expected relapse time drops to zero. This suggests that the bigger the primary tumor size is at resection, the faster relapse will occur.

https://doi.org/10.1371/journal.pcbi.1007423.g007

about 19 years the probability of only undetectable metastases present and the conditional mean relapse time both approach zero. Let us stress that while some clinical studies report data on the whole distribution of recurrence times, these are usually measured from a varying time of surgery, which corresponds to different primary tumor resection sizes. Therefore, unless the distribution of relapse times is reported together with the corresponding resection sizes, we cannot compare it directly to the predictions of our model. However, we expect the variability of primary sizes at resection to average out across large cohorts of patients, which is why we analyzed the expected value of the time to recurrence.

Using the values from Table 2 we tested our model by computing the probability of synchronous metastases and the mean relapse time conditioned on established but all undetectable metastases. The predictions from our model, typical ranges and references for each cancer type considered are summarized in Table 4. Notice that our predictions for the mean relapse time fall on the lower end of the respective typical ranges. This is expected since we compute the time to recurrence τ based on the minimal detectable size M, while in practice metastases are often detected only at larger sizes. In general, for different cancer types it is observed that metastases can grow up to 2 times faster than the primary tumor they originated from [24], although values as high as 4 have been proposed [95]. Our estimates fall within this range ($\lambda/\delta = 4$ for prostate cancer, 3 for lung and between 1.5 and 2 for the others). As per the time interval from primary onset to surgery, the typical range is 15 – 25 years [43]. The high variability

Table 4. Typical ranges of $P(S_T \geq 1)$ and $E[\tau - T|U_T]$, predicted value from the model and literature references for each cancer type.

Cancer type	Output	Range from clinical data	Theoretical prediction	Reference
Breast	$P(S_T \geq 1)$ (%)	5 – 10	6.13	[97–99]
	$E[\tau - T \mid U_T]$ (days)	590 – 1022	725	[100–102]
Colorectal	$P(S_T \geq 1)$ (%)	15 – 25	20.17	[99, 103–107]
	$E[\tau - T \mid U_T]$ (days)	353 – 760	356	[106–110]
Headneck	$P(S_T \geq 1)$ (%)	1 – 16.8	1.65	[111, 112]
	$E[\tau - T \mid U_T]$ (days)	219 – 623	435	[113–115]
Lung	$P(S_T \geq 1)$ (%)	30 – 55.39	33.96	[99, 116]
	$E[\tau - T \mid U_T]$ (days)	210 – 602	249	[117–119]
Prostate	$P(S_T \geq 1)$ (%)	10 – 34	13.53	[120–122]
	$E[\tau - T \mid U_T]$ (days)	730 – 1131	969	[123,124]

https://doi.org/10.1371/journal.pcbi.1007423.t004

in our estimates of DT_{pt} make T fall outside that range for headneck ($T = 7.69$y), lung ($T = 14.71$y) and prostate ($T = 32$y) cancers, classifying the first two as fast growing tumors and the latter as a slow growing one. The singular features that the model predicts for prostate cancer are in accordance with clinical studies (see e.g. [86, 96]).

The last trait of cancer recurrence that we are going to examine is disease-free rates. These generally correspond to the survival function of the relapse time, $\mathrm{P}(\tau > t)$. However, following the previous discussion we will condition this probability on no synchronous metastases, obtaining

$$\mathrm{P}(\tau \leq t \mid S_T = 0) = 1 - e^{-(b_t - b_T)} \tag{13}$$

for $t \geq T$. In this case we do not observe any convergence to the density without resection, because if $T \to 0$ then no metastasis can be initiated and if $T \to \infty$ the condition $S_T = 0$ pushes the relapse time to infinity. Let us also stress that our model does not provide information on survival rates, as no modelling of the time to decease is incorporated. Furthermore, notice that $P(\tau > t)$ yields a good description of the disease-free rates in terms of metastases detectability, but not necessarily with respect to cancer symptomaticity.

The relapse time distribution in case of no synchronous metastasis, $\mathrm{P}(\tau > t \mid \tau > T)$, for different resection times is shown in Fig 8, studying again the case of colorectal cancer. As we are not conditioning on at least one metastasis being initiated, there is always a positive probability that relapse will not occur, that is $\tau = \infty$. The resection times are thus chosen so to yield cure probabilities—$\mathrm{P}(K_T = 0)$, corresponding to the final plateaus—equal to 0.75, 0.6, 0.45, 0.3, 0.15 and 0.001, respectively. These times span across a total range of about 2.2 years. Furthermore, excluding the latest resection time considered, the difference between two consecutive of these T values is between 0.28 and 0.4 years. Hence, our model suggests that delays of the order of months in the time of primary resection can lead to a significant decrease in the cure probability.

To quantify more precisely the implications of surgery delays, we study the probability that the first metastasis is initiated in the time interval $(T, T + \Delta T)$

$$\mathrm{P}(K_{T+\Delta T} \geq 1, K_T = 0) = \mathrm{P}(K_{T+\Delta T} \geq 1) - \mathrm{P}(K_T \geq 1).$$

This probability is depicted in Fig 9 using our parameter estimates for colorectal cancer. We see in the figure that there is a middle range of resection sizes where the recurrence probability can be significantly affected by small surgery delays. For colorectal cancer we estimate that if the primary resection is originally planned for a tumor of diameter between 0.44 and 0.9

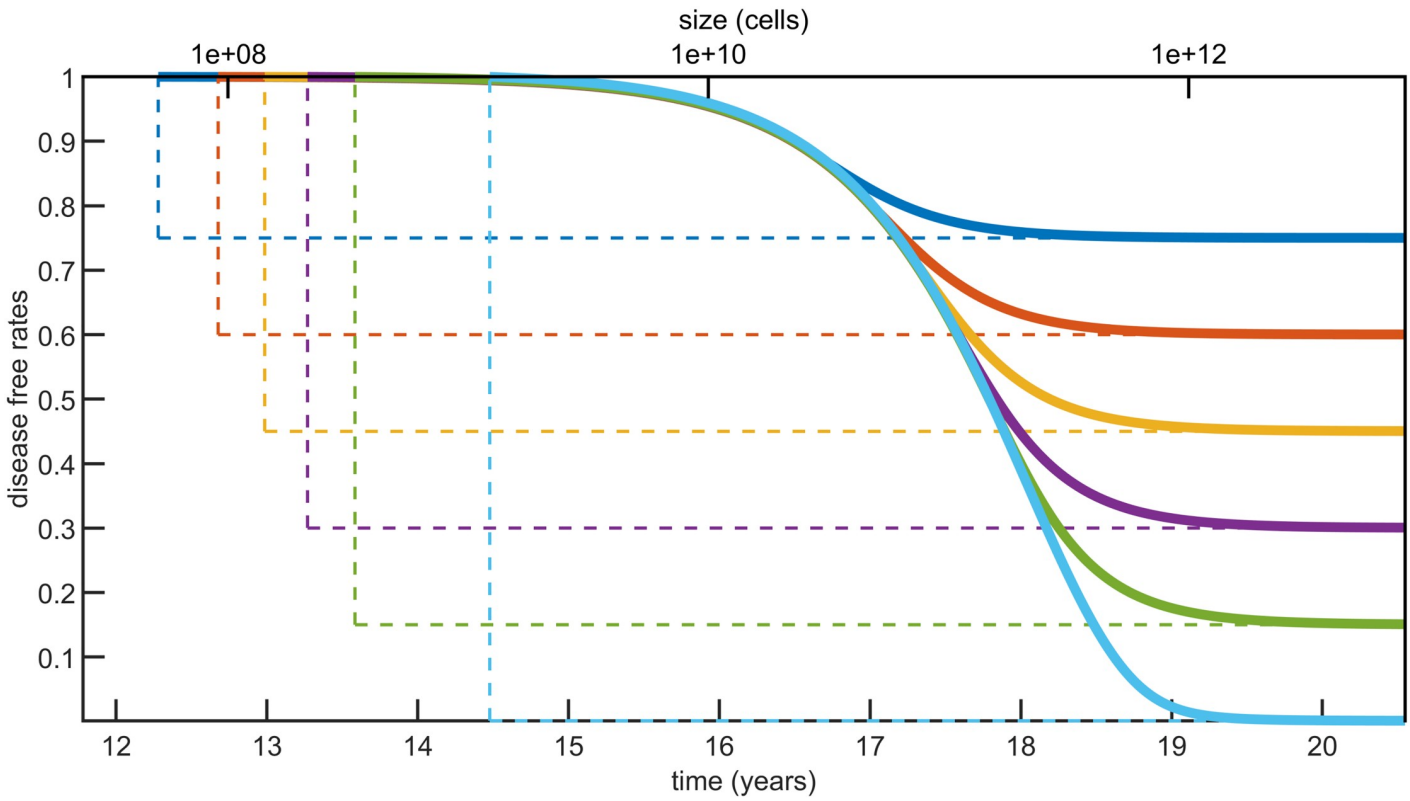

Fig 8. Disease-free curves for different resection times. The earlier the primary tumor is resected the higher is the probability that no metastases will arise, or cure probability, represented by the value of the final plateaus. The resection times are chosen so that $P(K_T = 0) = 0.75, 0.6, 0.45, 0.3, 0.15, 0.001$ respectively. With the parameter estimates for colorectal cancer (see Table 2) these times range from 12.28 to 14.48 years, corresponding to sizes between 5.12×10^7 and 1.23×10^9 cells (diameter 0.46 – 1.33cm), respectively.

https://doi.org/10.1371/journal.pcbi.1007423.g008

centimeters (4.39×10^7 and 3.89×10^8 cells, respectively), then a surgery delay of 60 days would decrease the cure probability by 5 – 9%. Conversely, tumors smaller than this critical range are less likely to metastasize during the surgery delay, while larger tumors likely metastasized already, so that the effect of surgery delay for these sizes is smaller.

Conclusions

We introduced a model of metastasis formation where metastases are initiated at a time dependent rate, in the simplest case proportional to the size of a growing primary tumor. All initiated metastases then evolve as independent supercritical branching processes. Parameters of the model were estimated for five different cancer types from the clinical literature. We studied the relapse time τ, that is the earliest time when any of the metastases becomes detectable. We obtained the distribution of τ for a general primary tumor growth and focused in particular on logistic and exponential growth functions. For clinically relevant initiation rates the metastases which relapse first are typically initiated in the early phase of the primary tumor development, which is exponential for both growth functions considered. Hence the distributions of τ for exponential and logistic primary growths are practically identical unless the initiation rate is unrealistically small ($\nu \approx 10^{-13}$ or smaller) and we can thus exploit the much simpler formulas for the exponentially growing tumor.

We model the resection of the primary tumor by introducing a cut-off for the growth function $n(t)$. If metastases are likely already established at surgery, their time of relapse is not

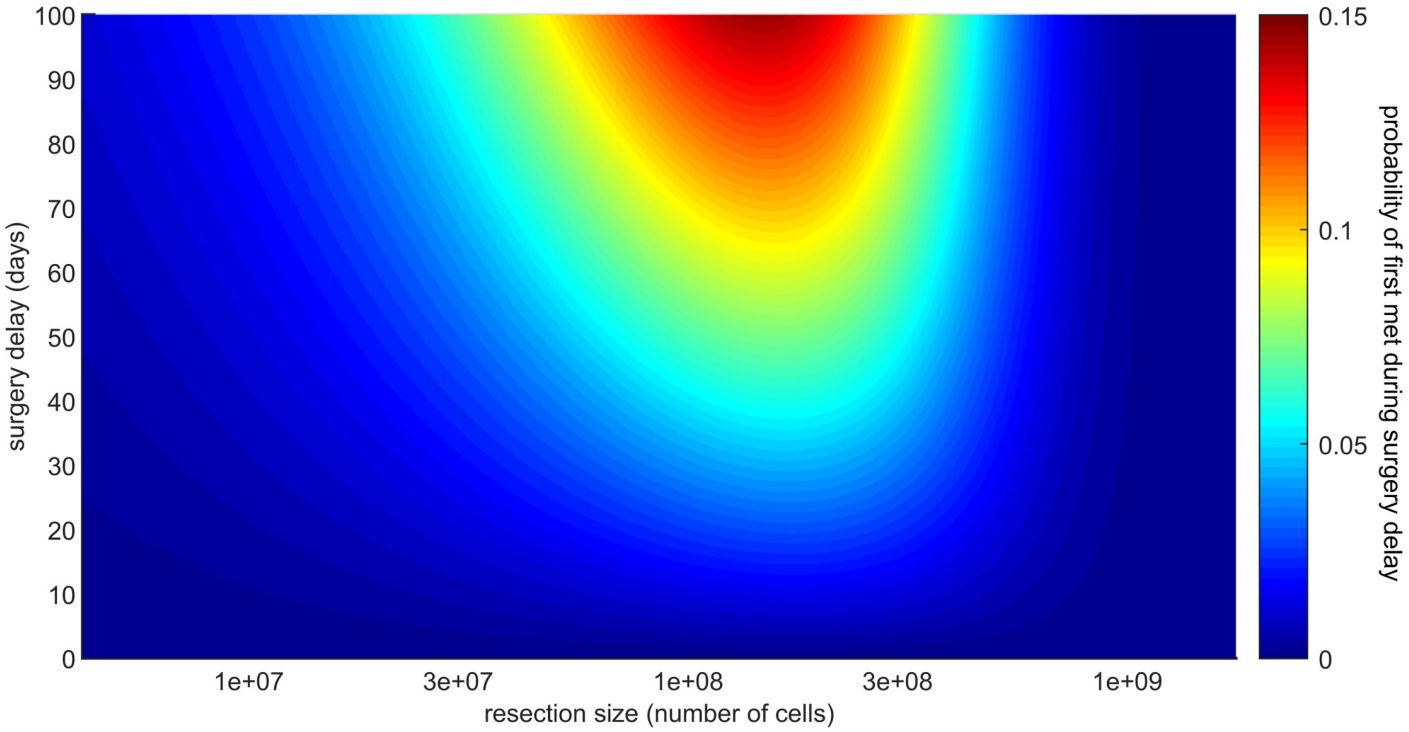

Fig 9. Probability of the first metastasis being initiated during surgery delay. This probability $P(K_{T+\Delta T} \geq 1, K_T = 0)$—where T is the set time of resection and ΔT the surgery delay—is plotted as a function of the resection size $N = e^{\delta T}$ (x-axis) and of the delay ΔT (y-axis). With the parameter estimates for colorectal cancer (see Table 2) we see that if a primary tumor is resected at a critical size (around 2×10^8 cells, diameter ≈ 0.725cm), surgery delays of 2-3 months can decrease the cure probability of more than 10%.

https://doi.org/10.1371/journal.pcbi.1007423.g009

influenced by the resection timing. We categorized all metastases into synchronous and metachronous and computed corresponding occurrence probabilities. With our estimated parameters we found that the probability of synchronous metastases and the mean relapse time after resection falls in the typical clinical range for all five different cancer types we study.

A challenging scenario for treatment is that of patients with established but all undetectable metastases. For all five cancer types we considered, the probability of this event is high within a significant range of resection sizes. Unfortunately, the typical size of a resected tumor falls in or near this range for all cancer types. We found that relatively small delays in these resection times can cause significant decrease in the cure probability. Within our model, surgery only prevents recurrence if it is done before the onset of the first surviving metastases.

The parameter estimates summarized in Table 2 yield realistic predictions for several quantities of clinical interest. Although in principle we can explore our model predictions across the whole range of parameters, this would often lead to unrealistic outcomes. In this sense the quantitative predictions of our model are quite sensitive to the parameter values, but we have been able to find a combination of parameters that yields realistic results. On the other hand, the qualitative features of our model are more robust to parameter changes, as demonstrated for example in Fig 6.

In particular, our estimate for the initiation rate of metastases, ν, is based on the assumption of early dissemination at primary size, $e^{\delta \mathrm{E}[\sigma_1]} = 10^8$ cells. However, since the metastatic net growth rate δ and extinction probability q are estimated independently from data on tumor volume doubling times (see Table 1), by changing the early dissemination assumption our model predictions could fall outside their typical ranges. For example, for colorectal cancer,

assuming $e^{\delta \mathrm{E}[\sigma_1]} = 10^9$ cells would lead to the unrealistic values $\mathrm{E}[\tau - T \mid U_T]$ = 836 days and $P(S_T \geq 1)$ = 2.23%. Thus, indirectly, our model supports the hypothesis of early metastatic dissemination.

Note that in this paper we focused on the presence or absence of synchronous or metachronous metastasis at resection as these events determine if there is ever a relapse ($K_T \geq 1$) or if relapse has already occurred by resection ($S_T \geq 1$). Our model also provides estimates for the number and sizes of metastases at resection, but these are less relevant for the study of the time to cancer relapse, and have already been studied in detail in [16, 29]. A general feature the model predicts is that the cumulative distribution of metastases sizes at resection has a power law tail with exponent δ/λ. This power law tail was observed in [16] using data on 21 patients with colorectal cancer from [13], and the exponent was found to typically be in the range 0.3 − 0.8. Our estimate δ/λ = 0.61 falls in this range, supporting our parameter inference. The paper above also reports data on the number of visible metastases at surgery. In our model, for a given primary resection size $e^{\delta T}$, this number is a Poisson random variable S_T. However, since the primary tumor sizes are not published and likely different for all patients in the data, we could not use this quantity reliably for our parameter estimation. For example, if we infer the initiation rate ν for colorectal cancer from the probability of visible metastasis at resection (given by $P(S_T \geq 1) = 1 - e^{-b_T}$ and with estimate 0.2 from the data reported in Table 4) we would get essentially the same estimate as in Table 2. But by using instead the mean number of visible metastases (expressed as $E(S_T|S_T \geq 1) = b_T/(1 - e^{-b_T})$, with estimated lower bound 1.4 from [107]), we would infer a 3 times greater estimate for ν. Again, a possible cause of this discrepancy lies in the different resection sizes for patients which we have no data for.

Metastases are seeded and establish colonies via a specific and complex process called metastatic cascade (for details see e.g. [125]). Since this is known to be a multi-stage process, some authors (see for example [6, 126, 127] and references therein) have described metastases initiation through two-type stochastic models, where a cell needs to gain the ability to metastasize before it can establish a new metastatic lesion. We did not choose that route for several reasons: (i) the precise details of how and when cells reach this ability are not clear [43, 128], (ii) in our model we can think of $n(t)$ as the number of cells which can metastasize and so tailor the two approaches, and (iii) if we assume that an acquired metastatic ability lowers the primary net growth rate and that the seeding rate is sufficiently small (at most 10^{-4} according to simulations), a branching process model would predict the same exponential growth for the cells with this ability [29, 129], and hence this would only change the estimate of the initiation rate in our model.

We did not include into our model a mechanism for metastases seeding other metastases, although this phenomenon has been observed in clinical studies [130]. The main reason for this omission was the lack of reliable data for the estimation of the secondary seeding rate. By assuming the same primary and secondary seeding rates, however, we would expect metastases to initiate secondary ones when they reach around 10^8 cells, at which size they are already detectable. Hence, by considering this scenario our predictions for the time to cancer relapse would not change.

We aim to compare our model in the future to data where relapse times are given jointly with primary tumor sizes at resection. Tumor size is of course not the only relevant factor in predicting relapse times, so the model should be extended to involve other features like a measure of malignancy, possibly as in [131]. Many of the parameters of the model can differ between patients, and also between each metastasis. Therefore, including a probability distribution for the parameters could also make our model more realistic, provided that such distributions can be estimated from data. Other possible extensions could include interactions

among metastatic cells and among metastatic lesions, effects of the immune system, allowing metastases to seed other metastases, and providing an estimate for the fraction of cells which can metastasize, perhaps through modelling angiogenesis.

Materials and methods

In this section we provide more details about the mathematical foundations of our model.

Single type process

Let $(Z_t)_{t\geq 0}$ be a birth-death branching process, i.e. a Markov chain on non-negative integers with transition rates

$$i \mapsto \begin{cases} i+1 & \text{rate } i\alpha \\ i-1 & \text{rate } i\beta \end{cases}$$

The two positive constants α and β are called birth and death rate, respectively. In our model we employ this process to describe the evolution of each metastasis. We assume that all metastases have the same birth and death rate and that they are supercritical, that is they have positive net growth rate $\lambda = \alpha - \beta > 0$. Moreover, since we only want to model surviving metastasis, we condition on the eventual survival of the process, that is on the event $\Omega_\infty = \{\omega: Z_t(\omega) > 0 \text{ for all } t \geq 0\}$. The probability of such event is equal to $P(\Omega_\infty) = 1 - q$, where $q = \beta/\alpha$ [31].

We define the first passage time to size M as $T_M := \inf\{t > 0: Z_t = M\}$. A well known property of branching processes is that $e^{-\lambda t} Z_t \to W$ almost surely as $t \to \infty$, and conditioned on survival and a single initial cell $W \sim \text{Expo}(\lambda/\alpha)$ [31]. Since W and T_M are connected by $\lim_{M\to\infty} Me^{-\lambda T_M} = W$, an immediate consequence is that

$$\mathrm{P}(T_M \leq t \mid \Omega_\infty \cap \{Z_0 = 1\}) \sim e^{-(1-q)Me^{-\lambda t}} \equiv G(t) \qquad \text{as } M \to \infty \tag{14}$$

Early derivations of this result already appear in [132, 133]. Interestingly, T_M follows the Gumbel distribution $\text{Gumb}_{\max}\left(\frac{\log M(1-q)}{\lambda}, \frac{1}{\lambda}\right)$, where

$$Y \sim \text{Gumb}_{\max}(a,b) \quad \Leftrightarrow \quad \mathrm{P}(Y \leq y) = e^{-e^{-\frac{y-a}{b}}}, \quad a \in \mathbb{R},\ b > 0$$

The Gumbel type is an extreme value distribution. If M_n denotes the maximum of n IID random variables X_i, the Gumbel distribution above generally describes the limit of M_n as $n \to \infty$, when X_i have an exponential (right) tail. A similar definition can be given for the reverse Gumbel distribution, i.e. the limit of minimum of IID random variables with an exponential (left) tail

$$Y \sim \text{Gumb}_{\min}(a,b) \quad \Leftrightarrow \quad \mathrm{P}(Y \leq y) = 1 - e^{-e^{\frac{y-a}{b}}}, \quad a \in \mathbb{R},\ b < 0$$

For both of these distributions we have

$$Y \sim \text{Gumb}(a,b) \quad \Rightarrow \quad \mathrm{E}[Y] = a + b\gamma_E, \quad \mathrm{Var}(Y) = \frac{\pi^2}{6} b^2 \tag{15}$$

where $\gamma_E \approx 0.5772$ denotes the Euler-Mascheroni constant. Hence the mean hittingtime to M

cells grows logarithmically with M, while its variance remains constant

$$\mathrm{E}[T_M] = \frac{\log M(1-q) + \gamma_E}{\lambda}, \quad \mathrm{Var}(T_M) = \frac{\pi^2}{6\lambda^2}$$

Thus, for sizes $M \approx \alpha/\lambda$ the standard deviation is approximately equal to the mean, but since the mean only grows logarithmically with M, fluctuations of T_M stay relevant even for much larger values of M.

Scaled relapse time distribution

In Results we derive the general expression for the relapse time distribution, whose full expression is obtained by combining Eqs 3, 4 and 14. Here we show how to scale the detectable size M out of this expression, so to split the distribution into a deterministic part and a stochastic term. Let us focus on the integral

$$\int_0^t n(s)G(t-s)ds = \int_0^t n(s)e^{-(1-q)Me^{-\lambda(t-s)}}ds$$

and apply the change of variables $z := t - s - \frac{1}{\lambda}\log M$ to find

$$\int_{-\frac{1}{\lambda}\log M}^{t-\frac{1}{\lambda}\log M} n\left(t - z - \frac{1}{\lambda}\log M\right)e^{-(1-q)e^{-\lambda z}}dz$$

By plugging this expression back into Eq 4, at time $t + \frac{1}{\lambda}\log M$ we get

$$\mathrm{P}\left(\tau - \frac{1}{\lambda}\log M \leq t\right) = 1 - \exp\left(-\nu(1-q)\int_{-\frac{1}{\lambda}\log M}^{t} n(t-z)e^{-(1-q)e^{-\lambda z}}dz\right)$$

Hence, as M tends to infinity we obtain

$$\tau - \frac{1}{\lambda}\log M \xrightarrow[M\to\infty]{d} \bar{\tau}$$

where

$$\mathrm{P}(\bar{\tau} \leq t) = 1 - e^{-\nu(1-q)\int_{-\infty}^{t} n(t-s)e^{-(1-q)e^{-\lambda s}}ds}$$

From the last two equations we also see that asymptotically as $M \to \infty$

$$\mathrm{E}[\tau] \sim \frac{1}{\lambda}\log M + C, \qquad C = \mathrm{E}[\bar{\tau}] \tag{16}$$

Explicit results for exponential primary growth

Two commonly employed growth functions for primary tumors are the exponential $n_e(t) = e^{\delta t}$ and the logistic $n_l(t) = \frac{Ke^{\delta t}}{K+e^{\delta t}-1}$ ones (see e.g. [33]). A logistic growth implies that the primary tumor has a carrying capacity K. During the first stages of its development $n_l(t)$ follows the same exponential trajectory of $n_e(t)$ and then approaches a constant as it gets closer to size K. As the carrying capacity is typically large, this slowdown for $n_l(t)$ happens around $\hat{t} = \log(K)/\delta$. The differences between the results provided by these two growths functions

thus depend on the probability of metastases being initiated by time $\hat{t}$, i.e. $P(K_{\hat{t}} \geq 1) \approx 1 - e^{-\frac{\nu(1-q)K}{\delta}}$. Hence, if

$$\frac{\nu(1-q)K}{\delta} \gg 1 \tag{17}$$

metastases are likely established in the first stages of the primary growth, i.e. when $n_l(t) \approx n_e(t)$. Otherwise, metastases are initiated late in the primary evolution, when the two growth functions are substantially different. This feature is visualized in Fig 2, where τ densities for a logistic growth are shown to converge to the exponential ones as ν increases and the other parameters are fixed.

Using the parameter values from Table 2, however, we observe that the condition in Eq 17 is satisfied for all cancer types considered. In other words, our estimates for ν, q, K and δ yield no difference between exponential and logistic growth functions. In light of this, we study in greater detail the results obtained with $n_e(t)$.

Scaled relapse time. When $n(t) = n_e(t) = e^{\delta t}$, the relapse time distribution has an expression in terms of special functions. To show this, let us consider the distribution of the scaled relapse time $\bar{\tau}$ as given by Eq 5 and focus on the integral

$$\int_{-\infty}^{t} n(t-s)e^{-(1-q)e^{-\lambda s}}ds = e^{\delta t}\int_{-\infty}^{t} e^{-(1-q)e^{-\lambda s}-\delta s}ds$$

This can be equivalently written as

$$e^{\delta t}\int_{-\infty}^{t} \frac{1}{(1-q)^{\delta/\lambda}}[(1-q)e^{-\lambda s}]^{\delta/\lambda}e^{-(1-q)e^{-\lambda s}}ds$$

The last expression then suggests the change of variable $x = (1-q)e^{-\lambda s}$, which leads to

$$\frac{e^{\delta t}}{\lambda(1-q)^{\delta/\lambda}}\int_{(1-q)e^{-\lambda t}}^{\infty} x^{\frac{\delta}{\lambda}-1}e^{-x}dx = \frac{e^{\delta t}}{\lambda(1-q)^{\delta/\lambda}}\Gamma\left(\frac{\delta}{\lambda},(1-q)e^{-\lambda t}\right)$$

and where Γ denotes the incomplete upper gamma function $\Gamma(a,t) = \int_t^{\infty} x^{a-1}e^{-x}dx$. The scaled relapse time distribution for $n(t) = e^{\delta t}$ is thus given by

$$P(\bar{\tau} \leq t) = 1 - \exp\left(-\frac{\nu(1-q)^{1-\frac{\delta}{\lambda}}e^{\delta t}}{\lambda}\Gamma\left(\frac{\delta}{\lambda},(1-q)e^{-\lambda t}\right)\right) \tag{18}$$

Since $\Gamma(1,t) = e^{-t}$, for $\lambda = \delta$ this simplifies to

$$P(\bar{\tau} \leq t) = 1 - \exp\left(-\frac{\nu}{\lambda}e^{-(1-q)e^{-\lambda t}+\lambda t}\right)$$

Small initiation limit. While the initiation rate can vary significantly across different cancer types, ν is typically orders of magnitude smaller then all other parameters. Hence, we now investigate τ distribution in the $\nu \to 0$ limit. Let us first consider the result given by Eq 18 for

the scaled time to recurrence $\bar{\tau}$ and write it as

$$\mathrm{P}(\bar{\tau} \leq t) = 1 - \exp\left(-\frac{\nu(1-q)^{1-\frac{\delta}{\lambda}}\Gamma\left(\frac{\delta}{\lambda}\right)e^{\delta t}}{\lambda}\right)\exp\left(\frac{\nu(1-q)^{1-\frac{\delta}{\lambda}}\phi(t)e^{\delta t}}{\lambda}\right) \tag{19}$$

where

$$\phi(t) = \int_0^{(1-q)e^{-\lambda t}} s^{\frac{\delta}{\lambda}-1}e^{-s}ds < \int_0^{(1-q)e^{-\lambda t}} s^{\frac{\delta}{\lambda}-1}ds = \frac{\lambda}{\delta}(1-q)^{\frac{\delta}{\lambda}}e^{-\delta t}$$

Notice that the second exponential factor in Eq 19 is bounded below by 1 and above by $e^{\frac{\nu(1-q)}{\delta}}$ for all $t \geq 0$. Therefore, as $\nu \to 0$, the distribution of $\bar{\tau}$ asymptotically converges to

$$\mathrm{P}(\bar{\tau} \leq t) \sim 1 - \exp\left(-\frac{\nu(1-q)^{1-\frac{\delta}{\lambda}}\Gamma\left(\frac{\delta}{\lambda}\right)e^{\delta t}}{\lambda}\right)$$

Equivalently, for small initiation rates the scaled relapse time $\bar{\tau}$ asymptotically follows a Gumbel distribution for the minimum, $\bar{\tau} \sim \mathrm{Gumb}_{\min}\left(-\frac{1}{\delta}\log\frac{\nu(1-q)^{1-\frac{\delta}{\lambda}}\Gamma(\frac{\delta}{\lambda})}{\lambda}, -\frac{1}{\delta}\right)$.

Mean relapse time. By combining the last result with Eqs 15 and 16 we find that

$$\mathrm{E}[\tau] \approx \frac{1}{\lambda}\log M + \frac{1}{\delta}\log\frac{\delta}{\nu} + C$$

where $C = -\frac{1}{\delta}\left(\log\frac{\delta(1-q)^{1-\frac{\delta}{\lambda}}\Gamma\left(\frac{\delta}{\lambda}\right)}{\lambda} + \gamma_E\right)$. Intuitively, the time to relapse is likely to be determined by one of the first established metastases. Given the simple dependence of $E[\tau]$ on M and ν, we now compare it with the mean time to detectability of the first metastasis, $E[\tau_1]$. Let us first recall that $\tau_1 = \sigma_1 + \Theta_1$ is equal to the sum of the first initiation time and the hitting time to M. As $\nu \to 0$, the distribution of the first arrival σ_1, given in general by $1 - e^{-a_t}$, converges to a reverse Gumbel with parameters $\frac{1}{\delta}\log\frac{\delta}{\nu(1-q)}$ and $-\frac{1}{\delta}$. This implies in particular that

$$\mathrm{E}[\sigma_1] = \frac{1}{\delta}\left(\log\frac{\delta}{\nu(1-q)} - \gamma_E\right) = \frac{1}{\delta}\log\frac{\delta}{\nu} + C_1$$

where $C_1 = -\frac{\log(1-q)+\gamma_E}{\delta}$. Moreover, the hitting times Θ_i follow the Gumbel distribution $G(t)$—see Eq 2—and hence

$$\mathrm{E}[\Theta_i] = \frac{1}{\lambda}\log M - C_2$$

for every i, where $C_2 = -\frac{\log(1-q)+\gamma_E}{\lambda}$. Joining the last two results we get

$$\mathrm{E}[\tau_1] = \mathrm{E}[\sigma_1 + \Theta_1] = \frac{1}{\lambda}\log M + \frac{1}{\delta}\log\frac{\delta}{\nu} + \tilde{C} \tag{20}$$

where $\tilde{C} = C_1 - C_2$. By comparing Eq 20 with the expression for $E[\tau]$, we notice indeed the same M and ν dependence, but the constants C and $\tilde{C}$ have different analytical forms.

Numerical computation. Finally, all the plots and computations reported in this paper have been performed on Matlab R2018b. The lines of code below provide an efficient way (in the example for the exponential case) to calculate the relapse time distribution given by Eq 4 for a vector of times `tspan`.

```
n = @(t)(exp(delta*t));
G = @(t)(exp(-(1-q)*M*exp(-lambda*t)));
F = @(t)(1-exp(-nu*(1-q)*integral(@(s)(n(s).*G(t-s)),0,t,'ArrayValued',true)));
x = arrayfun(@(t)F(t), tspan);
```

Acknowledgments

We thank Ivana Bozic, David Cheek, Jasmine Foo, Kevin Leder, Michael Nicholson and Johannes Reiter for helpful discussions.

Author Contributions

Conceptualization: Stefano Avanzini, Tibor Antal.

Investigation: Stefano Avanzini, Tibor Antal.

Writing – review & editing: Stefano Avanzini, Tibor Antal.

References

1. Sahai E. Illuminating the metastatic process. Nature Reviews Cancer. 2007; 7(10):737–749. https://doi.org/10.1038/nrc2229 PMID: 17891189
2. Naxerova K, Brachtel E, Salk JJ, Seese AM, Power K, Abbasi B, et al. Hypermutable DNA chronicles the evolution of human colon cancer. Proceedings of the National Academy of Sciences. 2014; 111(18):E1889–E1898. https://doi.org/10.1073/pnas.1400179111
3. Harper KL, Sosa MS, Entenberg D, Hosseini H, Cheung JF, Nobre R, et al. Mechanism of early dissemination and metastasis in Her2+ mammary cancer. Nature. 2016; 54
4. Reiter JG, Makohon-Moore AP, Gerold JM, Heyde A, Attiyeh MA, Kohutek ZA, et al. Minimal functional driver gene heterogeneity among untreated metastases. Science. 2018; 361(6406):1033–1037. https://doi.org/10.1126/science.aat7171 PMID: 30190408
5. Michor F, Nowak MA, Iwasa Y. Stochastic dynamics of metastasis formation. Journal of Theoretical Biology. 2006; 240(4):521–530. https://doi.org/10.1016/j.jtbi.2005.10.021 PMID: 16343545
6. Haeno H, Michor F. The evolution of tumor metastases during clonal expansion. Journal of Theoretical Biology. 2010; 263(1):30–44. https://doi.org/10.1016/j.jtbi.2009.11.005 PMID: 19917298
7. Chaffer CL, Weinberg RA. A Perspective on Cancer Cell Metastasis. Science. 2011; 331(6024):1559–1564. https://doi.org/10.1126/science.1203543 PMID: 21436443
8. Tsikitis VL, Larson DW, Huebner M, Lohse CM, Thompson PA. Predictors of recurrence free survival for patients with stage II and III colon cancer. BMC Cancer. 2014; 14(1). https://doi.org/10.1186/1471-2407-14-336 PMID: 24886281
9. Luria SE, Delbrück M. Mutations of bacteria from virus sensitivity to virus resistance. Genetics. 1943; 48(6):491–511.
10. Iwasa Y, Nowak MA, Michor F. Evolution of Resistance During Clonal Expansion. Genetics. 2006; 172(4):2557–2566. https://doi.org/10.1534/genetics.105.049791 PMID: 16636113
11. Komarova N. Stochastic modeling of drug resistance in cancer. Journal of Theoretical Biology. 2006; 239:351–366. https://doi.org/10.1016/j.jtbi.2005.08.003 PMID: 16194548
12. Foo J, Leder K. Dynamics of cancer recurrence. The Annals of Applied Probability. 2013; 23(4):1437–1468. https://doi.org/10.1214/12-AAP876
13. Bozic I, Reiter JG, Allen B, Antal T, Chatterjee K, Shah P, et al. Evolutionary dynamics of cancer in response to targeted combination therapy. eLife. 2013; 2. https://doi.org/10.7554/eLife.00747 PMID: 23805382

14. Durrett R, Moseley S. Evolution of resistance and progression to disease during clonal expansion of cancer. Theoretical Population Biology. 2010; 77:42–48. https://doi.org/10.1016/j.tpb.2009.10.008 PMID: 19896491

15. Durrett R, Foo J, Leder K, Mayberry J, Michor F. Evolutionary dynamics of tumor progression with random fitness values. Theoretical Population Biology. 2010; 78(1):54–66. https://doi.org/10.1016/j.tpb.2010.05.001 PMID: 20488197

16. Nicholson MD, Antal T. Universal Asymptotic Clone Size Distribution for General Population Growth. Bulletin of Mathematical Biology. 2016; 78(11):2243–2276. https://doi.org/10.1007/s11538-016-0221-x PMID: 27766475

17. Dingli D, Michor F, Antal T, Pacheco JM. The emergence of tumor metastases. Cancer Biology & Therapy. 2007; 6(3):383–390. https://doi.org/10.4161/cbt.6.3.3720

18. Armitage P, Doll R. The Age Distribution of Cancer and a Multi-stage Theory of Carcinogenesis; 1954.

19. Hanin LG, Tsodikov AD, Yakovlev AY. Optimal schedules of cancer surveillance and tumor size at detection. Mathematical and Computer Modelling. 2001; 33(12-13):1419–1430. https://doi.org/10.1016/S0895-7177(01)80023-6

20. Hanin L, Pavlova L. Optimal screening schedules for prevention of metastatic cancer. Statistics in Medicine. 2012; 32(2):206–219. https://doi.org/10.1002/sim.5474 PMID: 22807074

21. Tsodikov AD, Ibrahim JG, Yakovlev AY. Estimating Cure Rates From Survival Data. Journal of the American Statistical Association. 2003; 98(464):1063–1078. https://doi.org/10.1198/016221450300000001007 PMID: 21151838

22. Yakovlev AY. Threshold models of tumor recurrence. Mathematical and Computer Modelling. 1996; 23(6):153–164. https://doi.org/10.1016/0895-7177(96)00024-6

23. Yakovlev AY, Tsodikov AD, Asselain B. Stochastic Models of Tumor Latency and Their Biostatistical Applications. World Scientific; 1996.

24. Klein CA. Parallel progression of primary tumours and metastases. Nature Reviews Cancer. 2009; 9:302. https://doi.org/10.1038/nrc2627 PMID: 19308069

25. Lea DE, Coulson CA. The distribution of the numbers of mutants in bacterial populations. Journal of Genetics. 1949; 49(3):264–285. https://doi.org/10.1007/bf02986080 PMID: 24536673

26. Keller P, Antal T. Mutant number distribution in an exponentially growing population. Journal of Statistical Mechanics: Theory and Experiment. 2015;P01011. https://doi.org/10.1088/1742-5468/2015/01/P01011

27. Kendall DG. Birth-and-death processes, and the theory of carcinogenesis. Biometrika. 1960; 47:13–21. https://doi.org/10.2307/2332953

28. Kessler DA, Levine H. Scaling Solution in the Large Population Limit of the General Asymmetric Stochastic Luria–Delbrück Evolution Process. Journal of Statistical Physics. 2014; 158(4):783–805. https://doi.org/10.1007/s10955-014-1143-3

29. Cheek D, Antal T. Mutation frequencies in a birth–death branching process. The Annals of Applied Probability. 2018; 28(6):3922–3947. https://doi.org/10.1214/18-AAP1413

30. Tubiana M. The growth and progression of human tumors: Implications for management strategy. Radiotherapy and Oncology. 1986; 6(3):167–184. https://doi.org/10.1016/s0167-8140(86)80151-7 PMID: 3529254

31. Athreya KB, Ney PE. Branching Processes. Dover Publications; 2004.

32. Collins VP, Loeffler RK, Tivery H. Observations on growth rates of human tumors. The American journal of roentgenology, radium therapy, and nuclear medicine. 1956; 76:988–1000. PMID: 13362715

33. Preziosi L. Cancer Modelling and Simulation. Chapman & Hall/CRC Mathematical and Computational Biology. CRC Press, Taylor & Francis Group; 2003.

34. Bolognese A, Izzo L. Surgery in Multimodal Management of Solid Tumors. Springer Milan; 2009.

35. Peng Y, Taylor JMG. Cure Models. In: Handbook of Survival Analysis. Chapman & Hall; 2014. p. 113–134.

36. Allison PD. Survival analysis using SAS: a practical guide. 2nd ed. SAS Publishing; 2010.

37. Meeker WQ, Escobar LA. Statistical Methods for Reliability Data. John Wiley & Sons Inc.; 1998.

38. Singh R, Mukhopadhyay K. Survival analysis in clinical trials: Basics and must know areas. Perspectives in Clinical Research. 2011; 2(4):145. https://doi.org/10.4103/2229-3485.86872 PMID: 22145125

39. Hagar YC, Harvey DJ, Beckett LA. A multivariate cure model for left-censored and right-censored data with application to colorectal cancer screening patterns. Statistics in medicine. 2016; 35:3347–3367. https://doi.org/10.1002/sim.6934 PMID: 26990553

40. Adam R, de Gramont A, Figueras J, Kokudo N, Kunstlinger F, Loyer E, et al. Managing synchronous liver metastases from colorectal cancer: A multidisciplinary international consensus. Cancer Treatment Reviews. 2015; 41(9):729–741. https://doi.org/10.1016/j.ctrv.2015.06.006 PMID: 26417845

41. Schwartz M. A biomathematical approach to clinical tumor growth. Cancer. 1961; 14:1272–1294. https://doi.org/10.1002/1097-0142(196111/12)14:6<1272::aid-cncr2820140618>3.0.co;2-h PMID: 13909709

42. Spratt JS, Spratt TL. Rates of Growth of Pulmonary Metastases and Host Survival. Annals of Surgery. 1964; 159(2):161–171. https://doi.org/10.1097/00000658-196402000-00001 PMID: 14119181

43. Jones S, Chen Wd, Parmigiani G, Diehl F, Beerenwinkel N, Antal T, et al. Comparative lesion sequencing provides insights into tumor evolution. Proceedings of the National Academy of Sciences. 2008; 105(11):4283–4288. https://doi.org/10.1073/pnas.0712345105

44. Haustermans K, Fowler J, Geboes K, Christiaens MR, Lerut A, van der Schueren E. Relationship between potential doubling time (Tpot), labeling index and duration of DNA synthesis in 60 esophageal and 35 breast tumors: is it worthwhile to measure Tpot? Radiotherapy and Oncology. 1998; 46 (2):157–167. https://doi.org/10.1016/s0167-8140(97)00164-3 PMID: 9510043

45. Denekamp J. New Approaches to the Measurement of Proliferation Rates. Angiogenesis in Health and Disease. 1992; p. 333–337. https://doi.org/10.1007/978-1-4615-3358-0_31

46. Bertuzzi A, Gandolfi A, Sinisgalli C, Starace G, Ubezio P. Cell loss and the concept of potential doubling time. Cytometry. 1997; 29(1):34–40. https://doi.org/10.1002/(SICI)1097-0320(19970901)29:1%3C34::AID-CYTO3%3E3.0.CO;2-D PMID: 9298809

47. von Fournier D, Weber E, Hoeffken W, Bauer M, Kubli F, Barth V. Growth rate of 147 mammary carcinomas. Cancer. 1980; 45:2198–2207. https://doi.org/10.1002/1097-0142(19800415)45:8<2198::aid-cncr2820450832>3.0.co;2-7 PMID: 7370960

48. Kuroishi T, Tominaga S, Morimoto T, Tashiro H, Itoh S, Watanabe H, et al. Tumor Growth Rate and Prognosis of Breast Cancer Mainly Detected by Mass Screening. Japanese Journal of Cancer Research. 1990; 81(5):454–462. https://doi.org/10.1111/j.1349-7006.1990.tb02591.x PMID: 2116393

49. Peer PGM, Van Dijck JAAM, Verbeek ALM, Hendriks JHCL, Holland R. Age-dependent growth rate of primary breast cancer. Cancer. 1993; 71(11):3547–3551. https://doi.org/10.1002/1097-0142(19930601)71:11<3547::aid-cncr2820711114>3.0.co;2-c PMID: 8490903

50. Ryu EB, Chang JM, Seo M, Kim SA, Lim JH, Moon WK. Tumour volume doubling time of molecular breast cancer subtypes assessed by serial breast ultrasound. European Radiology. 2014; 24 (9):2227–2235. https://doi.org/10.1007/s00330-014-3256-0 PMID: 24895040

51. Förnvik D, Lång K, Andersson I, Dustler M, Borgquist S, Timberg P. Estimates of breast cancer growth rate from mammograms and its relation to tumour characteristics. Radiation Protection Dosimetry. 2015; 169(1-4):151–157. https://doi.org/10.1093/rpd/ncv417 PMID: 26410768

52. Zhang S, Ding Y, Zhou Q, Wang C, Wu P, Dong J. Correlation Factors Analysis of Breast Cancer Tumor Volume Doubling Time Measured by 3D-Ultrasound. Medical Science Monitor. 2017; 23:3147–3153. https://doi.org/10.12659/MSM.901566 PMID: 28652562

53. Kusama S, Spratt JS, Jr, Donegan WL, Watson FR, Cunningham C. The gross rates of growth of human mammary carcinoma. Cancer. 1972; 30(2):594–599. https://doi.org/10.1002/1097-0142(197208)30:2<594::aid-cncr2820300241>3.0.co;2-2

54. Friberg S, Mattson S. On the growth rates of human malignant tumors: implications for medical decision making. Journal of surgical oncology. 1997; 65:284–297. https://doi.org/10.1002/(sici)1096-9098(199708)65:4<284::aid-jso11>3.0.co;2-2 PMID: 9274795

55. Awwad H. Radiation Oncology: Radiobiological and Physiological Perspectives. Springer Netherlands; 2013.

56. Zabicki K, Colbert JA, Dominguez FJ, Gadd MA, Hughes KS, Jones JL, et al. Breast Cancer Diagnosis in Women $\leq$ 40 versus 50 to 60 Years: Increasing Size and Stage Disparity Compared With Older Women Over Time. Annals of Surgical Oncology. 2006; 13(8):1072–1077. https://doi.org/10.1245/ASO.2006.03.055

57. Lee SH, Kim YS, Han W, Ryu HS, Chang JM, Cho N, et al. Tumor growth rate of invasive breast cancers during wait times for surgery assessed by ultrasonography. Medicine. 2016; 95(37):e4874. https://doi.org/10.1097/MD.0000000000004874 PMID: 27631256

58. de l'Aulnoit AH, Rogoz B, Pinçon C, de l'Aulnoit DH. Metastasis-free interval in breast cancer patients: thirty-year trends and time dependency of prognostic factors. A retrospective analysis based on a single institution experience. The Breast. 2018; 37:80–88. https://doi.org/10.1016/j.breast.2017.10.008

59. Bolin S, Nilsson E, Sjödahl R. Carcinoma of the colon and rectum–growth rate.; 1983.

60. Tada M, Misaki F, Kawai K. Growth rates of colorectal carcinoma and adenoma by roentgenologic follow-up observations. Gastroenterologia Japonica. 1984; 19:550–555. https://doi.org/10.1007/bf02793869 PMID: 6526254

61. Choi SJ, Kim HS, Ahn SJ, Jeong YM, Choi HY. Evaluation of the growth pattern of carcinoma of colon and rectum by MDCT. Acta Radiologica. 2013; 54(5):487–492. https://doi.org/10.1177/0284185113475923 PMID: 23436826

62. Finlay IG, Meek D, Bruntont F, McArdle CS. Growth rate of hepatic metastases in colorectal carcinoma. British Journal of Surgery. 1988; 75(7):641–644. https://doi.org/10.1002/bjs.1800750707 PMID: 3416116

63. Tanaka K, Shimada H, Miura M, Fujii Y, Yamaguchi S, Endo I, et al. Metastatic Tumor Doubling Time: Most Important Prehepatectomy Predictor of Survival and Nonrecurrence of Hepatic Colorectal Cancer Metastasis. World Journal of Surgery. 2004; 28(3):263–270. https://doi.org/10.1007/s00268-003-7088-3 PMID: 14961200

64. Tomimaru Y, Noura S, Ohue M, Okami J, Oda K, Higashiyama M, et al. Metastatic Tumor Doubling Time Is an Independent Predictor of Intrapulmonary Recurrence after Pulmonary Resection of Solitary Pulmonary Metastasis from Colorectal Cancer. Digestive Surgery. 2008; 25(3):220–225. https://doi.org/10.1159/000140693 PMID: 18577868

65. Wilson MS, West CM, Wilson GD, Roberts SA, James RD, Schofield PF. Intra-tumoral heterogeneity of tumour potential doubling times (Tpot) in colorectal cancer. British journal of cancer. 1993; 68:501–506. https://doi.org/10.1038/bjc.1993.376 PMID: 8353040

66. Kornprat P, Pollheimer MJ, Lindtner RA, Schlemmer A, Rehak P, Langner C. Value of Tumor Size as a Prognostic Variable in Colorectal Cancer. American Journal of Clinical Oncology. 2011; 34(1):43–49. https://doi.org/10.1097/COC.0b013e3181cae8dd PMID: 20101166

67. Ding Z, Wang Z, Huang S, Zhong S, Lin J. Comparison of laparoscopic vs. open surgery for rectal cancer. Molecular and Clinical Oncology. 2017; 6(2):170–176. https://doi.org/10.3892/mco.2016.1112 PMID: 28357087

68. Waaijer A, Terhaard CHJ, Dehnad H, Hordijk GJ, van Leeuwen MS, Raaymakers CPJ, et al. Waiting times for radiotherapy: consequences of volume increase for the TCP in oropharyngeal carcinoma. Radiotherapy and Oncology. 2003; 66(3):271–276. https://doi.org/10.1016/s0167-8140(03)00036-7 PMID: 12742266

69. Jensen AR, Nellemann HM, Overgaard J. Tumor progression in waiting time for radiotherapy in head and neck cancer. Radiotherapy and Oncology. 2007; 84(1):5–10. https://doi.org/10.1016/j.radonc.2007.04.001 PMID: 17493700

70. Galante E, Gallus G, Chiesa F, Bono A, Bettoni I, Molinari R. Growth rate of head and neck tumors. European Journal of Cancer and Clinical Oncology. 1982; 18(8):707–712. https://doi.org/10.1016/0277-5379(82)90067-0 PMID: 6891321

71. Umino S, Hayashi S, Ono S. Doubling time of pulmonary metastases of adenoid cystic carcinoma. International Journal of Oral and Maxillofacial Surgery. 1997; 26: 48. https://doi.org/10.1016/S0901-5027(97)80987-3

72. Zackrisson B, Gustafsson H, Stenling R, Flygare P, Wilson GD. Predictive value of potential doubling time in head and neck cancer patients treated by conventional radiotherapy. International Journal of Radiation Oncology*Biology*Physics. 1997; 38(4):677–683. https://doi.org/10.1016/S0360-3016(97)00066-7

73. Muto M, Nakane M, Katada C, Sano Y, Ohtsu A, Esumi H, et al. Squamous cell carcinoma in situ at oropharyngeal and hypopharyngeal mucosal sites. Cancer. 2004; 101(6):1375–1381. https://doi.org/10.1002/cncr.20482 PMID: 15368325

74. Markou K, Goudakos J, Triaridis S, Konstantinidis J, Vital V, Nikolaou A. The role of tumor size and patient's age as prognostic factors in laryngeal cancer. Hippokratia. 2011; 15(21607041):75–80.

75. Kerr KM, Lamb D. Actual growth rate and tumour cell proliferation in human pulmonary neoplasms. British Journal Of Cancer. 1984; 50:343. https://doi.org/10.1038/bjc.1984.181 PMID: 6087867

76. Arai T, Kuroishi T, Saito Y, Kurita Y, Naruke T, Kaneko M. Tumor Doubling Time and Prognosis in Lung Cancer Patients: Evaluation from Chest Films and Clinical Follow-up Study. Japanese Journal of Clinical Oncology. 1994.

77. Detterbeck FC, Gibson CJ. Turning Gray: The Natural History of Lung Cancer Over Time. Journal of Thoracic Oncology. 2008; 3(7):781–792. https://doi.org/10.1097/JTO.0b013e31817c9230 PMID: 18594326

78. Henschke CI, Yankelevitz DF, Yip R, Reeves AP, Farooqi A, Xu D, et al. Lung Cancers Diagnosed at Annual CT Screening: Volume Doubling Times. Radiology. 2012; 263(2):578–583. https://doi.org/10.1148/radiol.12102489 PMID: 22454506

79. Yoo H, Nam BH, Yang HS, Shin SH, Lee JS, Lee SH. Growth rates of metastatic brain tumors in non-small cell lung cancer. Cancer. 2008; 113(5):1043–1047. https://doi.org/10.1002/cncr.23676 PMID: 18618515

80. Fowler JF. Biological Factors Influencing Optimum Fractionation in Radiation Therapy. Acta Oncologica. 2001; 40(6):712–717. https://doi.org/10.1080/02841860152619124 PMID: 11765065

81. Bando T. A new method of segmental resection for primary lung cancer: intermediate results. European Journal of Cardio-Thoracic Surgery. 2002; 21(5):894–899. https://doi.org/10.1016/s1010-7940(02)00122-7 PMID: 12062282

82. Strand TE. Survival after resection for primary lung cancer: a population based study of 3211 resected patients. Thorax. 2006; 61(8):710–715. https://doi.org/10.1136/thx.2005.056481 PMID: 16601091

83. D'Amico AV, Hanks GE. Linear regressive analysis using prostate-specific antigen doubling time for predicting tumor biology and clinical outcome in prostate cancer. Cancer. 1993; 72:2638–2643. https://doi.org/10.1002/1097-0142(19931101)72:9<2638::aid-cncr2820720919>3.0.co;2-n PMID: 7691393

84. Werahera PN, Glode LM, Rosa FGL, Lucia MS, Crawford ED, Easterday K, et al. Proliferative Tumor Doubling Times of Prostatic Carcinoma. Prostate Cancer. 2011; 2011:1–7. https://doi.org/10.1155/2011/301850

85. Zharinov GM, Bogomolov OA, Neklasova NN, Anisimov VN. Pretreatment prostate specific antigen doubling time as prognostic factor in prostate cancer patients. Oncoscience. 2017; 4:7–13. https://doi.org/10.18632/oncoscience.337 PMID: 28484728

86. Berges RR, Vukanovic J, Epstein JI, CarMichel M, Cisek L, Johnson DE, et al. Implication of cell kinetic changes during the progression of human prostatic cancer. Clinical cancer research: an official journal of the American Association for Cancer Research. 1995; 1:473–480.

87. Haustermans KMG, Hofland I, Poppel HV, Oyen R, de Voorde WV, Begg AC, et al. Cell kinetic measurements in prostate cancer. International Journal of Radiation Oncology*Biology*Physics. 1997; 37(5):1067–1070. https://doi.org/10.1016/S0360-3016(96)00579-2

88. Renshaw AA, Richie JP, Loughlin KR, Jiroutek M, Chung A, D'Amico AV. Maximum diameter of prostatic carcinoma is a simple, inexpensive, and independent predictor of prostate-specific antigen failure in radical prostatectomy specimens. Validation in a cohort of 434 patients. American journal of clinical pathology. 1999; 111:641–644. https://doi.org/10.1093/ajcp/111.5.641 PMID: 10230354

89. Johnson SB, Hamstra DA, Jackson WC, Zhou J, Foster B, Foster C, et al. Larger Maximum Tumor Diameter at Radical Prostatectomy Is Associated With Increased Biochemical Failure, Metastasis, and Death From Prostate Cancer After Salvage Radiation for Prostate Cancer. International Journal of Radiation Oncology*Biology*Physics. 2013; 87(2):275–281. https://doi.org/10.1016/j.ijrobp.2013.05.043

90. Serres S, Soto MS, Hamilton A, McAteer MA, Carbonell WS, Robson MD, et al. Molecular MRI enables early and sensitive detection of brain metastases. Proceedings of the National Academy of Sciences. 2012; 109(17):6674–6679. https://doi.org/10.1073/pnas.1117412109

91. Fujiwara S, Yao K, Nagahama T, Uchita K, Kanemitsu T, Tsurumi K, et al. Can we accurately diagnose minute gastric cancers ($\leq$5 mm)? Chromoendoscopy (CE) vs magnifying endoscopy with narrow band imaging (M-NBI). Gastric Cancer. 2015; 18(3):590–596. https://doi.org/10.1007/s10120-014-0399-2

92. Wang L. Early Diagnosis of Breast Cancer. Sensors. 2017; 17(7):1572. https://doi.org/10.3390/s17071572

93. Chignola R, Foroni RI. Estimating the Growth Kinetics of Experimental Tumors From as Few as Two Determinations of Tumor Size: Implications for Clinical Oncology. IEEE Transactions on Biomedical Engineering. 2005; 52(5):808–815. https://doi.org/10.1109/TBME.2005.845219 PMID: 15887530

94. Fillon M. Better Guidelines Needed for Cancer Survivorship Management. CA: A Cancer Journal for Clinicians. 2018; 68(6):392–393.

95. Lee SP, Sun JR, Qian H, McBride WH, Withers HR. Characterization of Metastatic Tumor Formation by the Colony Size Distribution. arXiv pre-print. 2006;.

96. Schmid HP, McNeal JE, Stamey TA. Observations on the doubling time of prostate cancer. The use of serial prostate-specific antigen in patients with untreated disease as a measure of increasing cancer volume. Cancer. 1993; 71(6):2031–2040. https://doi.org/10.1002/1097-0142(19930315)71:6<2031::aid-cncr2820710618>3.0.co;2-q PMID: 7680277

97. Andre F, Slimane K, Bachelot T, Dunant A, Namer M, Barrelier A, et al. Breast Cancer With Synchronous Metastases: Trends in Survival During a 14-Year Period. Journal of Clinical Oncology. 2004; 22(16):3302–3308. https://doi.org/10.1200/JCO.2004.08.095 PMID: 15310773

98. Boutros C, Mazouni C, Lerebours F, Stevens D, Lei X, Gonzalez-Angulo AM, et al. A preoperative nomogram to predict the risk of synchronous distant metastases at diagnosis of primary breast cancer. British Journal of Cancer. 2015; 112(6):992–997. https://doi.org/10.1038/bjc.2015.34 PMID: 25668007

99. Yilmaz U, Marks LB. Estimating changes in the rate of synchronous and metachronous metastases over time: Analysis of SEER data. Advances in Radiation Oncology. 2018; 3(1):70–75. https://doi.org/10.1016/j.adro.2017.09.007 PMID: 29556583

100. Kim H, Choi DH, Park W, Huh SJ, Nam SJ, Lee JE, et al. Prognostic factors for survivals from first relapse in breast cancer patients: analysis of deceased patients. Radiation Oncology Journal. 2013; 31(4):222. https://doi.org/10.3857/roj.2013.31.4.222 PMID: 24501710

101. Fitzpatrick DJ, Lai CS, Parkyn RF, Walters D, Humeniuk V, Walsh DCA. Time to Breast Cancer Relapse Predicted By Primary Tumour Characteristics, Not Lymph Node Involvement. World Journal of Surgery. 2013; 38(7):1668–1675. https://doi.org/10.1007/s00268-013-2397-7

102. Nowikiewicz T, Wiśniewska M, Wiśniewski M, Biedka M, Głowacka I, Kozak D, et al. Overall survival and disease-free survival in breast cancer patients treated at the Oncology Centre in Bydgoszcz—analysis of more than six years of follow-up. Współczesna Onkologia. 2015; 4:284–289.

103. Kemeny MM, Adak S, Gray B, Macdonald JS, Smith T, Lipsitz S, et al. Combined-Modality Treatment for Resectable Metastatic Colorectal Carcinoma to the Liver: Surgical Resection of Hepatic Metastases in Combination With Continuous Infusion of Chemotherapy—An Intergroup Study. Journal of Clinical Oncology. 2002; 20(6):1499–1505. https://doi.org/10.1200/JCO.2002.20.6.1499

104. Park JH, Kim TY, Lee KH, Han SW, Oh DY, Im SA, et al. The beneficial effect of palliative resection in metastatic colorectal cancer. British Journal Of Cancer. 2013; 108:1425. https://doi.org/10.1038/bjc.2013.94 PMID: 23481187

105. Lykoudis PM, O'Reilly D, Nastos K, Fusai G. Systematic review of surgical management of synchronous colorectal liver metastases. Br J Surg. 2014; 101(6):605–612. https://doi.org/10.1002/bjs.9449 PMID: 24652674

106. Elferink MAG, de Jong KP, Klaase JM, Siemerink EJ, de Wilt JHW. Metachronous metastases from colorectal cancer: a population-based study in North-East Netherlands. International Journal of Colorectal Disease. 2015; 30(2):205–212. https://doi.org/10.1007/s00384-014-2085-6 PMID: 25503801

107. Holch JW, Demmer M, Lamersdorf C, Michl M, Schulz C, von Einem JC, et al. Pattern and Dynamics of Distant Metastases in Metastatic Colorectal Cancer. Visceral Medicine. 2017; 33(1):70–75. https://doi.org/10.1159/000454687 PMID: 28612020

108. Hohenberger P, Schlag PM, Gerneth T, Herfarth C. Pre- and postoperative carcinoembryonic antigen determinations in hepatic resection for colorectal metastases. Predictive value and implications for adjuvant treatment based on multivariate analysis. Annals of Surgery. 1994; 219:135–143. https://doi.org/10.1097/00000658-199402000-00005 PMID: 8129484

109. Nordlinger B, Van Cutsem E, Gruenberger T, Glimelius B, Poston G, Rougier P, et al. Combination of surgery and chemotherapy and the role of targeted agents in the treatment of patients with colorectal liver metastases: recommendations from an expert panel. Annals of Oncology. 2009; 20(6):985–992. https://doi.org/10.1093/annonc/mdn735 PMID: 19153115

110. Sturesson C, Valdimarsson VT, Blomstrand E, Eriksson S, Nilsson JH, Syk I, et al. Liver-first strategy for synchronous colorectal liver metastases—an intention-to-treat analysis. HPB. 2017; 19(1):52–58. https://doi.org/10.1016/j.hpb.2016.10.005

111. Ferlito A, Shaha AR, Silver CE, Rinaldo A, Mondin V. Incidence and Sites of Distant Metastases from Head and Neck Cancer. ORL. 2001; 63(4):202–207. https://doi.org/10.1159/000055740 PMID: 11408812

112. Jain KS, Sikora AG, Baxi SS, Morris LGT. Synchronous cancers in patients with head and neck cancer. Cancer. 2013; 119(10):1832–1837. https://doi.org/10.1002/cncr.27988 PMID: 23423883

113. Liu SA, Wong YK, Lin JC, Poon CK, Tung KC, Tsai WC. Impact of recurrence interval on survival of oral cavity squamous cell carcinoma patients after local relapse. Otolaryngology-Head and Neck Surgery. 2007; 136(1):112–118. https://doi.org/10.1016/j.otohns.2006.07.002 PMID: 17210345

114. Ebrahimi A, Clark JR, Ahmadi N, Palme CE, Morgan GJ, Veness MJ. Prognostic significance of disease-free interval in head and neck cutaneous squamous cell carcinoma with nodal metastases. Head & Neck. 2012; 35(8):1138–1143. https://doi.org/10.1002/hed.23096

115. Wiegand S, Zimmermann A, Wilhelm T, Werner JA. Survival After Distant Metastasis in Head and Neck Cancer. Anticancer research. 2015; 35:5499–5502. PMID: 26408715

116. Tönnies M, Pfannschmidt J, Bauer TT, Kollmeier J, Tönnies S, Kaiser D. Metastasectomy for Synchronous Solitary Non-Small Cell Lung Cancer Metastases. The Annals of Thoracic Surgery. 2014; 98(1):249–256. https://doi.org/10.1016/j.athoracsur.2014.03.028 PMID: 24820385

117. al Kattan K, Sepsas E, Fountain SW, Townsend ER. Disease recurrence after resection for stage I lung cancer. European journal of cardio-thoracic surgery: official journal of the European Association for Cardio-thoracic Surgery. 1997; 12:380–384. https://doi.org/10.1016/S1010-7940(97)00198-X

118. Hung JJ, Jeng WJ, Hsu WH, Wu KJ, Chou TY, Hsieh CC, et al. Prognostic factors of postrecurrence survival in completely resected stage I non-small cell lung cancer with distant metastasis. Thorax. 2010; 65(3):241–245. https://doi.org/10.1136/thx.2008.110825 PMID: 20335294

119. Farsi AA, Swaminath A, Ellis P. Patterns of Relapse in Small Cell Lung Cancer (SCLC): A Retrospective Analysis of Outcomes from a Single Canadian Center. Journal of Thoracic Oncology. 2017; 12(1): S727–S728. https://doi.org/10.1016/j.jtho.2016.11.962

120. Koo KC, Yoo H, Kim KH, Park SU, Han KS, Rha KH, et al. Prognostic Impact of Synchronous Second Primary Malignancies on the Overall Survival of Patients with Metastatic Prostate Cancer. Journal of Urology. 2015; 193(4):1239–1244. https://doi.org/10.1016/j.juro.2014.10.088 PMID: 25444987

121. F PA Jr, Nehra A, Parker W, Wyre H, Mirza M, Duchene DA, et al. Metastatic prostate cancer in the modern era of PSA screening. International braz j urol. 2017; 43(3):416–421. https://doi.org/10.1590/s1677-5538.ibju.2016.0340

122. Almeida PL, Pereira BJ. Local treatment of metastatic prostate cancer: what is the evidence so far? Prostate Cancer. 2018; 2018:1–7. https://doi.org/10.1155/2018/2654572

123. Boorjian SA, Thompson RH, Tollefson MK, Rangel LJ, Bergstralh EJ, Blute ML, et al. Long-Term Risk of Clinical Progression After Biochemical Recurrence Following Radical Prostatectomy: The Impact of Time from Surgery to Recurrence. European Urology. 2011; 59(6):893–899. https://doi.org/10.1016/j.eururo.2011.02.026 PMID: 21388736

124. Toussi A, Stewart-Merrill SB, Boorjian SA, Psutka SP, Thompson RH, Frank I, et al. Standardizing the Definition of Biochemical Recurrence after Radical Prostatectomy—What Prostate Specific Antigen Cut Point Best Predicts a Durable Increase and Subsequent Systemic Progression? Journal of Urology. 2016; 195(6):1754–1759. https://doi.org/10.1016/j.juro.2015.12.075

125. Obenauf AC, Massagué J. Surviving at a Distance: Organ-Specific Metastasis. Trends in Cancer. 2015; 1(1):76–91. https://doi.org/10.1016/j.trecan.2015.07.009 PMID: 28741564

126. Durrett R. Branching process models of cancer. vol. 1.1 of Stochastics in biological systems. 1st ed. Springer International Publishing; 2015.

127. Haeno H, Gonen M, Davis MB, Herman JM, Iacobuzio-Donahue CA, Michor F. Computational Modeling of Pancreatic Cancer Reveals Kinetics of Metastasis Suggesting Optimum Treatment Strategies. Cell. 2012; 148(1-2):362–375. https://doi.org/10.1016/j.cell.2011.11.060 PMID: 22265421

128. Yachida S, Jones S, Bozic I, Antal T, Leary R, Fu B, et al. Distant metastasis occurs late during the genetic evolution of pancreatic cancer. Nature. 2010; 467:1114. https://doi.org/10.1038/nature09515 PMID: 20981102

129. Nicholson MD, Antal T. Competing evolutionary paths in growing populations with applications to multidrug resistance. PLOS Computational Biology. 2019; 15(4):e1006866. https://doi.org/10.1371/journal.pcbi.1006866 PMID: 30986219

130. Gundem G, Loo PV, Kremeyer B, Alexandrov LB, Tubio JMC, et al. The evolutionary history of lethal metastatic prostate cancer. Nature. 2015; 520(7547):353–357. https://doi.org/10.1038/nature14347 PMID: 25830880

131. Bozic I, Antal T, Ohtsuki H, Carter H, Kim D, Chen S, et al. Accumulation of driver and passenger mutations during tumor progression. Proceedings of the National Academy of Sciences. 2010; 107(43):18545–18550. https://doi.org/10.1073/pnas.1010978107

132. Williams T. The Basic Birth-Death Model for Microbial Infections. Journal of the Royal Statistical Society Series B (Methodological). 1965; 27(2):338–360. https://doi.org/10.1111/j.2517-6161.1965.tb01501.x

133. Waugh WAO. Uses of the sojourn time series for Markovian birth process. In: Proceedings of the Sixth Berkeley Symposium on Mathematical Statistics and Probability, Volume 3: Probability Theory. Berkeley, CA: University of California Press; 1972. p. 501–514.